

LOW CYCLE FATIGUE BEHAVIOUR OF AISI 308 STAINLESS STEEL WELD METAL

A thesis submitted in partial fulfilment of the requirements for the degree of

Master of Technology (Research)

In

Metallurgical and Materials Engineering



Submitted by

Abhishek Chaturvedi

Roll No. 610MM302

Department of Metallurgical and Materials Engineering

National Institute of Technology Rourkela

Rourkela-769008

2013

LOW CYCLE FATIGUE BEHAVIOUR OF AISI 308 STAINLESS STEEL WELD METAL

A thesis submitted in partial fulfilment of the requirements for the degree of

Master of Technology (Research)

In

Metallurgical and Materials Engineering



Submitted by

Abhishek Chaturvedi

Roll No. 610MM302

Under the Guidance of

Prof. B B Verma

Department of Metallurgical & Materials Engineering,
National Institute of Technology Rourkela
Rourkela -769008

Dr. S SIVAPRASAD (Principle Scientist)

Materials Science & Technology Division,
National Metallurgical Laboratory
Jamshedpur- 831007

Dedicated

To

My Family & Friends



**National Institute Of Technology
Rourkela**

CERTIFICATE

This is to certify that the thesis entitled, “**Low Cycle Fatigue Behaviour of AISI 308 Stainless Steel Weld Metal**” submitted by **Mr. ABHISHEK CHATURVEDI** in partial fulfilment of the requirements for the award of Master of Technology (Research) Degree in **METALLURGICAL AND MATERIALS ENGINEERING** with specialization in “**METALLURGICAL AND MATERIALS ENGINEERING**” at the National Institute of Technology, Rourkela is an authentic work carried out by him under our supervision and guidance.

To the best of our knowledge, the matter embodied in the thesis has not been submitted to any other University / Institute for the award of any Degree or Diploma.

Prof. B. B. Verma
Dept. of Metallurgical and Materials Engg.
National Institute of Technology
Rourkela-769008

Dr. S. Sivaprasad (Principle Scientist)
Materials Science & Technology Division
National Metallurgical Laboratory
Jamshedpur- 831007

Date:

Place:

ACKNOWLEDGEMENT

The satisfaction and euphoria that accompany the successful completion of a task would be incomplete without the mention of the people who made it possible and whose constant guidance and encouragement crowned all the efforts with success.

Therefore, I would like to take this opportunity to express my sincere and heartfelt gratitude to all those who made this report possible.

At first I would like to thank My Guide, Thesis supervisor **Prof B.B.Verma** Department of Metallurgical & Materials Engineering, National Institute of Technology, Rourkela who permits me to work at National Metallurgical Laboratory, Jamshedpur. Without his support and invaluable guidance, it is impossible for me to complete this work.

I bow humbly to record my deep sense of gratitude to My Co-Supervisor **Dr. S. Sivaprasad** Principle Scientist, National Metallurgical Laboratory Jamshedpur, who always motivate me and enlighten me with his valuable suggestions. With his constant encouragement and able guidance during every stage of the work that brought the research to a successful completion.

I express my sincere gratitude to **Dr. S. Tarafder**, Deputy Director, National Metallurgical Laboratory, Jamshedpur, for his kind gesture in permitting me to carry out the present work at NML, Jamshedpur.

I thank **Prof. B.C.Ray** Head of the Department Metallurgical and Materials Engineering, National Institute of Technology, Rourkela, to carry out this project work at NML.

I am very thankful to **Prof. Krishna Dutta**, Department of Metallurgical and Materials Engineering, National Institute of Technology, Rourkela for helping me in thesis writing and providing valuable suggestions. I am also thankful to **Prof P K Ray**, Department of Mechanical Engineering for encouragement and helping me to select courses and identify research topic

I am also grateful to **Dr. N Parida, Dr. H N Bar, Dr. J K Sahu and Mr. Arpan Das** National Metallurgical Laboratory, Jamshedpur, for encouraging, providing research facilities, helping me in analyzing data and supporting during this investigation.

I would also like to acknowledge **Bhabha Atomic Research Centre**, Mumbai for funding the project and supplying material for investigation.

I thank my beloved juniors at NML Jamshedpur **Mr.Rachit Sarin** and **Mr.Bijoy Kumar Purohit**, who made my stay color full.

My sincere regards to, my friends at NML Jamshedpur, IIT Kharagpur and NIT Rourkela like **Kaustav Barat, Anindya Das, Siddharth Tiwari, Srikar Potnuru, Vaneshwar Sahu** and **D.Narismhachary**, for their co-operation during the period of work.

At last but not the least I thank my **Parents and Family Members** without whom support and motivation I cannot complete this work.

Abhishek Chaturvedi

M.Tech

(Metallurgical & Materials Engineering)

Contents

Title Page	
Dedication	
Certificate	
Acknowledgement	
Contents	
List of Figures	
List of Tables	
List of Symbols	
List of Abbreviations	
Abstract	

Chapter 1

1.0	Introduction	1-4
1.1	Introduction	2
1.2	Objective of the present work	3
1.3	Scope of the present work	3
1.4	Layout of the thesis	4

Chapter 2

2.0	Literature review	5-31
2.1	Introduction	6
2.2	Nuclear reactor and piping materials	6
2.3	Dissimilar metal weld (DMW)	7
	2.3.1. Types of DMW	7
	2.3.2. Application of DMW	8
	2.3.3. Mechanism of dissimilar metal joint failure	8
	2.3.4. Precautions to minimize failure	9
2.4	Fatigue in metallic materials	12
	2.4.1. Cyclic loading on materials	12
	2.4.1.1. Fatigue failure mechanism	13

2.4.1.2. Types of cyclic loadings	15
2.4.1.3. Factors affecting fatigue life	16
2.4.2. Material response to cyclic deformation	17
2.4.2.1. Bauschinger effect (Stress strain anisotropy)	17
2.4.2.2. Hardening softening Behaviour	18
2.4.2.3. Mean stress relaxation	20
2.4.2.4. Ratcheting	20
2.4.3. Loop Analysis	20
2.4.3.1. Cyclic stress strain curve (CSSC)	20
2.4.3.2. Masing / non Masing behaviour	23
2.4.3.3. Master curve	24
2.4.3.4. Plastic strain energy	25
2.4.4. Different approaches for predicting fatigue life	26
2.4.4.1. Stress based approach	26
2.4.4.2. Strain based approach	27
2.4.4.3. Energy based approach	29
2.4.5 Fatigue life estimation models	30
2.4.5.1. Walker parameter	30
2.4.5.2. SWT lifing equation	30
2.5 Summary	31

Chapter 3

3.0 Materials and methods	32-37
3.1 Introduction	33
3.2 Experimental procedure	33
3.2.1 Material	33
3.2.2 Chemical composition	34
3.2.3 Optical microscopy	34
3.2.4 Hardness measurement	34
3.2.5 Tensile test	34
3.2.6 Low cycle fatigue	35
3.2.7 Fractography	37

Chapter 4

4.0 RESULTS AND DISCUSSIONS	38-56
4.1 Introduction	39
4.2 Basic characterization of material	39
4.2.1. Chemical composition	39
4.2.2. Microstructural evaluation	39

	4.2.3. Hardness behaviour of material	40
4.3	Tensile deformation of weld SS 308	41
	4.3.1 Engineering stress strain behaviour of weld SS308	41
	4.3.2 True stress strain behaviour of weld SS 308	41
	4.3.3. Fractographic analysis of post tensile specimens'	42
4.4	Cyclic deformation behaviour of weld SS 308	43
	4.4.1. Bauschinger effect	43
	4.4.2. Cyclic hardening softening behaviour	45
	4.4.3 Variation of Loop shape parameter	46
	4.4.4. Stability in cyclic stress and strain	47
	4.4.5. Coffin Mansion plot	48
	4.4.6. Variation of total energy with strain amplitude	49
	4.4.7. Cyclic stress strain curve	49
	4.4.8. Comparison of MSSC and CSSC	50
	4.4.9. Masing / non Masing behaviour	51
	4.4.10. Master curve	52
	4.4.11 Variation of Plastic energy with strain amplitude	53
	4.4.12 Fatigue life estimation	54
	4.4.12.1. Walker model	54
	4.4.12.2. Smith Watson Topper (SWT) model	54
	4.4.13 Fractography of fatigue specimen	55

Chapter 5

	5.0 Concl usions and scope for future work	57-58
5.1	Conclusions	58
5.2	Scope for future work	58
	References	59-62
	Biodata	63-64

List of Figures

Figure 2. 1 Figure showing (a) MHTP of AHWR (b) DMW joint in AHWR.....	8
Figure 2. 2 Schematic representation of striation formation during fatigue crack growth.	14
Figure 2. 3 Schematic representations of the various stages of fatigue crack growth.....	15
Figure 2. 4 (a) completely reversed stress cycle (b) asymmetric stress cycle (c) Random stress cycle.	16
Figure 2. 5 Schematic representation of Bauschinger effect	18
Figure 2.6 Schematic response to various cyclic input variables (Dieter 1998).....	19
Figure 2. 7 Primary quantities of a hysteresis loop.	22
Figure 2. 8 Comparison of CSSC and MSSC curve illustrating cyclic hardening and cyclic softening respectively.....	22
Figure 2. 9 Schematic representation of transient cyclic deformation processes.....	23
Figure 2. 10 Schematic representation of (a) Masing behaviour (branco 2012) (b) non Masing behaviour (Paul 2011)	24
Figure 2. 11 Typical master curve.....	25
Figure 2. 12 Plastic strain energy calculation (a) Masing material (right) (b) Non Masing material (left).....	26
Figure 2. 13 Schematic representation of S N curve	27
Figure 2. 14 Schematic representation of Coffin Mansion plot.	28
Figure 2. 15 Total strain energy approach	30
Figure 3. 1 Schematic representation of welded block.....	33
Figure 3. 2 Orientation and specimen preparation plan through pipe (a) Side view (b) Top view	35
Figure 3. 3 Tensile subsize weld specimen. All dimensions are in ‘mm’	35
Figure 3. 4 Schematic diagram depicting flat sub size room temperature fatigue specimen.....	36
Figure 3. 5 Typical wave form used for low cycle fatigue test.....	36
Figure 3. 6 Typical hysteresis loops as generated during experiment.....	37

Figure 4. 1 Weld zone microstructure in different orientation (a) RC, (b) LC, (c) LR	40
Figure 4. 2 Engineering stress strain curve for weld SS 308	41
Figure 4. 3 True stress strain curve for weld SS 308	42
Figure 4. 4 Fractograph of post tensile weld SS 308 specimen	42
Figure 4. 5 Schematic diagram depicting Bauschinger effect	43
Figure 4. 6 Bauchinger strain.....	44
Figure 4. 7 Bauchinger stress.....	44
Figure 4. 8 Cyclic hardening softening behaviour	45
Figure 4. 9 Degree of Hardening	46
Figure 4. 10 Effect of loop shape parameter on fatigue life.	47
Figure 4. 11 Cyclic stability curve	48
Figure 4. 12 Coffin Mansion plot.....	48
Figure 4. 13 Variation of energy absorption with fatigue life	49
Figure 4. 14 Cyclic stress strain curve	50
Figure 4. 15 Comparison of cyclic and monotonic stress strain curve.....	51
Figure 4. 16 Non Masing behaviour of material	52
Figure 4. 17 (a) Master curve for weld SS 308 and (b) calculation of parameters from master curve.....	53
Figure 4. 18 (a) Comparison of CPSE and EPSE (b) Comparison with respect to strain amplitude	53
Figure 4. 19 Walker model for predicting life	54
Figure 4. 20 SWT model for fatigue life prediction.....	55
Figure 4. 21 Fractographs of post fatigued fracture surfaces at various strain amplitudes.....	55

List of Tables

Table 2. 1 Typical nuclear materials in service (Miteva taylor 2006)	7
Table 2. 2 Review of published literature correlating different microstructural properties with different welding parameters	10
Table 2. 3 Factors affecting fatigue life.....	16
Table 3. 1 Summary of low cycle fatigue tests	37
Table 4. 1 Chemical composition of the material.....	39
Table 4. 2 Ferrite volume fraction in weld SS	40
Table 4. 3 Average hardness values in weld zone	41
Table 4. 4 Tensile properties of weld SS 308	41
Table 4. 5 Stable loop for different strain amplitudes.....	47
Table 4. 6 Comparison of walker and SWT equivalent stress.....	55

List of Symbols

E	Modulus of elasticity
K	Strain hardening coefficient
n	Strain hardening exponent
K'	Cyclic strain hardening coefficient
n'	Cyclic strain hardening exponent
σ_f	Fatigue strength coefficient
b	Fatigue strength exponent
f	Fatigue ductility coefficient
c	Fatigue ductility exponent
N_f	Number of cycles to failure
σ_m	Mean stress

H Hardening factor

H_e Hardening factor for strain controlled experiment

H_s Hardening factor for stress controlled experiment

List of abbreviations

AHWR Advanced heavy water reactors

AISI American Iron and Steel Institute

ASME American Society of Mechanical Engineers

ASS Austenitic stainless steel

ASTM American Society for Testing and Materials

BWR Boiling Water Reactor

CPSE- Calculated plastic strain energy

CSSC- Cyclic stress strain curve

DMW Dissimilar Metal Weld

EPSE- Experimentally determined plastic strain energy

HCF High cycle fatigue

LCF Low cycle fatigue

LSP Loop shape parameter

MHTP Main heat transport piping system

MSSC- Monotonic stress strain curve

PWR Pressurized Water reactor

SEM Scanning electron microscope

SS Stainless steel

TEM Transmission electron microscope

UTS Ultimate tensile strength

YS Yield strength

ABSTRACT

Dissimilar metal welds (DMW) are widely employed to meet various fabrication requirements in the integrated structures. In advanced heavy water reactors (AHWR), main heat transport (MHT) piping system is made of austenitic stainless steels (SS) and the later part of the piping is often made of carbon steels mainly to reduce the overall cost of the structure. These two metals (austenitic and carbon steels) are joined by DMW using SS 308 electrode. The operating temperature of this structure varies from 25-285 °C. This fluctuation in temperature causes thermally induced elastic-plastic strain reversals.

In the present investigation an attempt has been made to study the low cycle fatigue (LCF) behaviour of AISI 308 stainless steel weld metal. All LCF tests were conducted at ambient condition following the ASTM standard E-606[1]. These tests were conducted at strain amplitudes of 0.5%, 0.7%, 1.0%, 1.2% and 1.5% under fully reversed cycles ($R=-1$).

Various approaches such as (i) strain, (ii) energy, (iii) cyclic stress-strain curve (CSSC) and (iv) master curve have been employed in this investigation[2]. Walker and Smith Watson Topper (SWT) life estimation models have also been attempted in the present study[3]. The experimental results indicate pronounced Bauschinger effect, softening during lower strain amplitudes and Non Masing behaviour. Comparison of cyclic stress-strain curve (CSSC) and monotonic stress strain curve (MSSC) shows complex hardening-softening behaviour. It is also known that plastic strain ($\Delta\epsilon_p$) is the predominant cause of energy dissipation during low cycle fatigue[4]. The plastic strain energy calculated from the experimental data and estimated using constitutive equation follows linear relationship with strain amplitude. This however remains constant when plotted as a function of number of cycles to failure. The observations exhibit that Walker and SWT fatigue life prediction models hold well in predicting fatigue life of the present material.

Key words: Dissimilar metal weld, Plastic strain energy, Low cycle fatigue, Weld SS308, Cyclic stress strain curve

Chapter 1

1.0 Introduction

1.1 Introduction

1.2 Objectives of the present work

1.3 Scope of the work

1.4 Layout of the thesis

Chapter 1

Introduction

1.1 Introduction

Nuclear energy is a clean, safe, reliable and competitive source of energy and can satisfy the needs of industrial civilization, aspirations of the developing nations and replace a significant part of the fossil fuels responsible for greenhouse gases. At present, nuclear power plants provide about 6% of the world's energy and only 1% of energy requirements of this nation [5]. The various advantages of nuclear energy often overshadowed by concerns related to design and safety of nuclear power plants. Therefore structural integrity of the encompassing components especially containing complex designs and joining processes are always a cause of concern for the designers. Dissimilar Metal Welding (DMW) is widely used joining process in these reactors. In nuclear power plants such welds are necessary for connecting austenitic stainless steel pipes to ferritic or plain carbon steel components [6]. These are used in safety class systems of all Pressurized Water Reactor (PWR) and Advanced Heavy Water Reactor (AHWR) plants [6]. Austenitic stainless steels are often employed in these conditions because of their good high temperature mechanical properties whereas plain carbon steels are used mainly for the purpose of cost reduction. Many structural components in nuclear power plants experience cyclic plasticity due to thermal reversals during startup and shut down operations. These welds are exposed to temperatures ranging from room temperature to as high as 823 K and pressure up to 100 MPa. The weld zone of these structures are often considered as the weakest link and cyclic deformation/ fracture behaviour of these structures are influenced by their presence [7]. The importance of cyclic plastic deformation and fracture has attracted extensive research in last two decades [8][9][10]. In their recent studies Pavethan *et al.* studied high cycle fatigue behaviour of medium carbon and austenitic stainless steel welds and reported *S-N* curves of the materials [8]. Sivaprasad *et al.* investigated the low cycle fatigue and crack growth behaviour of

austenitic stainless steel and plain carbon steel weld and reported Coffin Manson plot and Paris law parameters for the materials [10]. However, energy based approach, Masing/ non Masing behaviour, comparison of cyclic stress-strain curve (CSSC) and monotonic stress strain curve (MSSC) for SS 308 weld metal are not available in literature. The present investigation is dedicated to characterize the low cycle fatigue behaviour of SS 308 weld metal and study its above mentioned behaviour.

1.2 Objective of the present work

The main objective of the present investigation is to study and investigate the low cycle fatigue characterization of AISI 308 weld metal.

1.3 Scope of the work

The major scope of the work can be broadly summarized as:

(I) To characterize microstructures and to determine mechanical properties of the weld zone SS 308 stainless steel:

This part consists of (a) chemical composition analysis of the investigated material, (b) microstructural examination and measurement of grain size, and (c) determination of their hardness and tensile properties.

(II) To study the Low cycle fatigue behaviour of weld metal SS 308.

The major experiments to fulfil this objective are (a) strain controlled low cycle fatigue experiments are conducted at various strain amplitudes (b) examination of the micro mechanisms for fatigue damage using various fatigue analysis approaches.

(III) Fractographic examinations on fractured samples using scanning electron microscopy.

Fractographic examination of fracture surface using SEM to study the various features and to understand the mechanism involved in the fatigue failure of this metal.

1.4 Layout of the thesis

This thesis consists of five chapters. The requirement of related experiments along with significance of the problem is described in Chapter-1. Literature background related to fatigue behaviour of metal with special attention to DMW is presented in Chapter-2. The present study has been inspired by the achievements of the previous investigations and available gaps in this field. Details of various experimental procedures related to chemical composition analysis, microstructure analysis, hardness, tensile and low cycle fatigue are discussed in Chapter 3. The results obtained from the investigation along with detailed discussion are discussed in Chapter 4. Conclusions drawn from this work are summarized in Chapter-5 together with some proposed future work related to this area. All references cited throughout are compiled at the end of thesis in reference section.

Chapter 2

- 2.0 Literature review**
- 2.1 Introduction**
- 2.2 Nuclear reactor and piping materials**
- 2.3 Dissimilar metal weld (DMW)**
 - 2.3.1. Types of DMW**
 - 2.3.2. Applications of DMW**
 - 2.3.3. Mechanisms of dissimilar metal joint failure**
 - 2.3.4. Precautions to minimize failure**
- 2.4 Fatigue in metallic materials**
 - 2.4.1. Cyclic loading on materials**
 - 2.4.1.1. Fatigue failure mechanism**
 - 2.4.1.2. Types of cyclic loadings**
 - 2.4.1.3. Factors affecting fatigue life**
 - 2.4.2. Material response to cyclic deformation**
 - 2.4.2.1. Bauschinger effect (Stress strain anisotropy)**
 - 2.4.2.2. Hardening softening behaviour**
 - 2.4.2.3. Mean stress relaxation**
 - 2.4.2.4. Ratcheting**
 - 2.4.3. Loop Analysis**
 - 2.4.3.1. Cyclic stress strain curve (CSSC)**
 - 2.4.3.2. Masing / non Masing behaviour**
 - 2.4.3.3. Master curve**
 - 2.4.3.4. Plastic strain energy**
 - 2.4.4. Different approaches for predicting fatigue life**
 - 2.4.4.1. Stress based approach**
 - 2.4.4.2. Strain based approach**
 - 2.4.4.3. Energy based approach**
 - 2.4.5 Fatigue life estimation models**
 - 2.4.5.1. Walker parameter**
 - 2.4.5.2. SWT lifing equation**
- 2.5 Summary**

Chapter 2

Literature review

2.1 Introduction

It is by now well perceived that research related to low cycle fatigue behaviour of DMW materials is of adequate academic as well as practical importance. Investigations related to mechanical behaviour of DMW materials has been accelerated in the last decade of the past century. This chapter deals with reported work on fatigue behaviour including low cycle fatigue of various metals and dissimilar metal welds. However literature related to fatigue behaviour of weldment is limited. It is therefore seemed prerequisite to do a survey of work done so far and material systems studied under fatigue behaviour of DMW. A brief review of earlier work is incorporated in different sections of this chapter to enhance the basic understanding of the topic. Different materials in service of nuclear and other pressure vessel piping's are discussed in section 2.2. Brief introduction to DMW, their applications, its failure mechanism and prevention are reported in section 2.3. Cyclic deformation behaviour of metallic materials, different approaches towards them and various phenomena involved are discussed in section 2.4. A summary of the topics discussed in this chapter is presented in section 2.5 along with the design of the current research problem on the basis of previously reported literature.

2.2 Nuclear reactor and pressure vessel piping materials

The ever expanding demands of energy have increased our dependence on various nuclear, thermal and other types of power generation systems. These advanced power generation systems create more stringent service conditions (high temperature and pressure) which triggers the quest for higher and more energy efficient material with better thermal, mechanical and anti-corrosive properties. The vast fraternity of materials is available for selection but economic constraint and fabricability issues put further limitations on design engineers. Steel is widely used as piping material in various

pressure vessel systems due to its relative low cost and vast experience which has been acquired from its extensive use over time. For example, stainless steels like austenitic, ferritic, martensitic and duplex; special structural steels like SA 508, SA533 steels; different micro alloyed steels like Mn-Mo-Ni alloy steel, Mn-V-Ni alloy steel, Cr-Mo alloy steel etc. are in use as per the ASME Pressure Vessel and Boiler Code[11]. Traditionally, austenitic stainless steels have been used in the higher temperature regions of piping systems due to their good creep strength, thermal expansion coefficients, ease of fabrication and their excellent oxidation and corrosion resistance due to higher chromium contents which stabilize the austenite phase field and also combine with oxygen to form a protective oxide layer on the surface. Table 2.1 reports the typical materials (structural and stainless steels grades) present in service,

Table2. 1 Typical nuclear materials in service [6]

Material	Part used	Operating conditions	Standard
SA 508 Cl. 2	Nozzle materials	350°C, 15 MPa	ASME
SA 508 Cl 3	Nozzle materials	285°C, 15 MPa	ASME
SS 304	Piping material	350°C, 15 MPa	ASME
SS 304 LN	Piping material	350°C, 15 MPa	ASME
SS 316	Piping material	350°C, 15 MPa	ASME
SS 316 L	Piping material	350°C, 15 MPa	ASME
SA 333	Piping material	350°C, 15 MPa	ASME
SS 309	Filler material	350°C, 15 MPa	ASME
SS 308	Filler material	350°C, 15 MPa	ASME

2.3 Dissimilar metal weld

Welding is a most common phenomenon for joining of metals. DMW is a kind of process used to join different materials. This approach is used when transition in mechanical properties or other performance related parameters are required. In general joining of different materials is more difficult because it requires adequate knowledge of physical, chemical, mechanical and other performance parameters of all the included materials. Furthermore the choice of filler materials is more difficult due to its compatibility issues with base materials. [6][12].

2.3.1 Types of DMW

Various types of DMW are described in this section.

1. Two different materials joined together directly.

2. Two materials joined after buttering one of these with a layer of suitable material.
3. Two materials are joined by placing a transition piece between them.
4. Cladding of two materials (One material is coated by another material for a particular property enhancement purpose).[12]

2.3.2 Applications of DMW

DMW joints are extensively used in nuclear power plants, thermal power plants and other pressure vessel piping due to their cost effectiveness, enhanced anti corrosive and elevated temperature properties. Figure 2.1(a) shows main heat transport piping system (MHTP) of advanced heavy water reactor (AHWR) and 2.1(b) describes a typical DMW joint between ASS and plain carbon steel. Main steam pipes and heavy water carrying pipes of AHWR contains DMW joint between ASS and low alloy steel. Frequently, ASS piping is often used to contain high-temperature steam in power generation plants, but below a certain temperature and pressure, low alloy steels can be applied for the purpose[12].

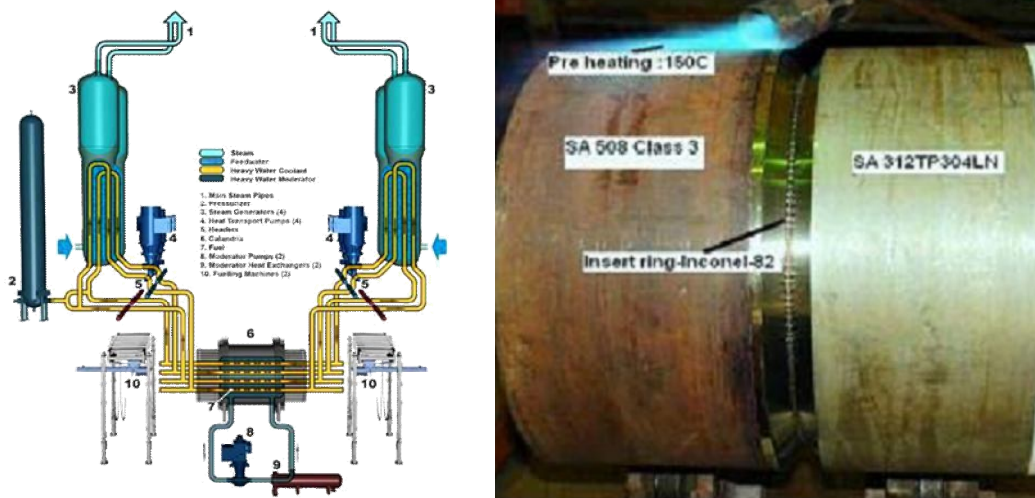


Figure 2. 1 Figure showing (a) MHTP of AHWR (b) DMW joint in AHWR. [10]

2.3.3 Mechanism of DMW joint failure

Integrity of DMW joints are always a cause of concern for engineers. Most of the literature regarding failure analysis of DMW corresponds to austenitic-ferritic and ferritic-

Ni welds. There is no particular cause or mechanism which can be made responsible for failure of these joints. However, three main features of failures can be categorized as.

1. Formation of an oxide notch.

Many of the austenitic-ferritic weld joints failed because of an oxide notch formed at the interface of weld and ferritic material. The reasons for this notch formation are different in different literatures. Klueh and King attributed this to loss of chromium or chromium carbide precipitation from ferritic matrix[13]. Vishwanathan and Diner pointed out that stress concentration due to change in strength at interfaces is a probable cause of oxide notch formation[13].

2. Cracking of prior austenite grain boundaries.

In case of stainless steel fillers creep cavitation in carbides may occur at prior austenite grain boundaries. This mode may associate with carbon depletion zone and differences in the thermal expansion coefficients.

3. Cracking of weld interface

In case of Ni based fillers, service conditions may generate carbides along the fusion line and cracking may occur in this zone. This may happen because of decarburized zone in ferrite region[13].

Apart from above mentioned mechanisms, a few other notable mechanisms of weld failures are hot cracking and weld decay of ASS weld joints, stress relief cracking, lamellar tearing in steels, delayed cracking by hydrogen and local brittle zone[14].

2.3.4 Precautions to minimize failure of DMW

Although there is no known method reported in the literature which can ensure integrity of DMW zone completely due to its complex nature, still apart from safe design consideration, reduction in carbon migration using buttering of suitable materials and reduction in thermal stresses by using materials with comparable thermal expansion coefficients may reduce the risk of failure up to certain extent. Table 2.2 reports the some important literature available in published domain regarding mechanical behavior of DMW majority of them are related to several grades of ASS, HSLA and other structural steels.

Table2. 2 Review of published literature correlating different microstructural properties with different welding parameters

Ref No.	Author	Year	System	Major findings
[15]	Kuwabara K <i>et al.</i>	1992	ASS-ferritic stainless steel	Fatigue strength decreases due to strain non uniformity caused by difference in cyclic plastic deformation across the weld.
[16]	Nelson T <i>et al.</i>	1999	ASS-ferritic stainless steel	Microstructure of base and weld significantly influences the nature and evaluation of fusion boundary at elevated temperatures.
[17]	Celik A <i>et al.</i>	1999	ASS-ferritic stainless steel	Steep increase in hardness was observed in HAZ of DMW weld in comparison to all ASS weld. Failure takes place at interface of ASS and weld metal interface and was trans granular ductile in nature.
[18]	Laha K <i>et al.</i>	2001	2.25Cr-1Mo/Alloy 800 DMW	Both the similar and dissimilar weld joints showed lower creep rupture life than base metal. The differences in the rupture lives between the base metal and the weld joint increased with a decrease in applied stress.
[19]	Bhandhari S <i>et al.</i>	2001	ASS-ferritic stainless steel	DMW of (ferritic/austenitic), subjected to an accidental transient and simulate using SYSTUS and shows simulation and experimental result within 5 % window.
[20]	Faidy C <i>et al.</i>	2003	Low alloy steel -ASS	Residual stresses are measured using neutron diffraction technique and shows higher amount in HAZ of SA 508.
[21]	Kusko CS <i>et al.</i>	2004	ASS 316L and AL6XN austenitic	Large grain sizes in both the weld metal and base metal produce a rough fracture surface that leads to improved fatigue resistance.
[22]	Keehan A <i>et al.</i>	2004	Steels	Strength increases were attributed to the formation of greater amounts of Martensite within the microstructure.
[23]	Kaskar R <i>et al.</i>	2004	Martensitic – Austenitic SS	Although, the pitting corrosion resistance of the all weld metal and weldment which was obtained with E308L-16 filler metal slightly better than weld made with E2209-17 filler metal due to higher level of austenite and reduced chromium nitride precipitation.
[24]	Ravi S <i>et al.</i>	2004	HSLA	1 The fatigue crack growth behaviour and fatigue life of the welded joints is influenced by mismatch ratio. 2 Mismatch ratio is inversely proportional relationship with fatigue crack growth exponent (m) and directly proportional relationship with threshold stress intensity factor (ΔK_{th}) and critical stress intensity factor (ΔK_{cr}).
[25]	Lee DG <i>et al.</i>	2004	Heat resistant steel STR and STS	The effect of notch position was investigated and the results were as follows: the nearer welds interface, the higher fatigue lives.

[26]	Shireesha M <i>et al.</i>	2005	ASS-ferritic stainless steel	Precipitation at the weld metal/ferritic steel interface occurs after 5000 hours of aging at 898 K but not for shorter durations. No decarburized zone was observed on the ferritic steel side even after 5000 hours of exposure.
[27]	Cui Y <i>et al.</i>	2005	ASS weld	Microfissures greatly decrease the fatigue properties of 316L austenitic stainless steel weld metals.
[28]	Satyanarayan V V <i>et al.</i>	2005	ASS-ferritic stainless steel	The toughness and strength properties of dissimilar metal welds are better than ferritic stainless steel parent metal.
[29]	Reddy G M <i>et al.</i>	2005	ASS-ferritic stainless steel	<p>1. The strength of dissimilar metal friction welds is intermediate to electron beam welds and gas tungsten arc welds, while the friction welds exhibited the highest toughness among all the dissimilar welds.</p> <p>2. ASS-ASS electron beam welds exhibited the highest strength and toughness due to fine solidification structure.</p> <p>3. Hardness and residual stresses are maximum on the ferritic stainless steel side of the interface in dissimilar metal fusion welds.</p> <p>4 Hardness and residual stress are maximum on the austenitic stainless steel side of the interface for dissimilar metal friction welds.</p>
[30]	DuPont JN <i>et al.</i>	2007	ASS-ferritic stainless steel	Ferritic-to-austenitic DMW made with Ni-based filler metals will exhibit a steeper concentration gradient in the partially mixed zone (PMZ) compared to Fe-based austenitic alloys.
[31]	Kim JS <i>et al.</i>	2007	Low alloy steel -ASS	SA508 base metals have higher yield strength and ultimate strength than alloy 82/182 weld and TP316 while the ultimate strengths of alloy 82/182 welds are similar as those of SA508 and SS316 base metals.
[32]	Jang C <i>et al.</i>	2008	Low alloy steel -ASS	The dendritic structures are well developed in Inconel 82/182 weld. Within the area between the dendrites, significant segregation and secondary phase precipitations are observed.
[33]	Kim J W <i>et al.</i>	2009	ASS-ferritic stainless steel	Significant gradients of the YS and UTS were observed within the HAZ of SA508 Gr.1a. This was attributed to the different microstructures within the HAZ resulting from the phase transformation during welding. However, the welding effect dominated the YS rather than UTS in the HAZ
[34]	Krishnaprasad K <i>et al.</i>	2009	ASS-Low alloy steel	Weld metal exhibited lower crack growth rate at intermediate ΔK region and CS region showed the highest rate.
[35]	Abadhi M M H <i>et al.</i>	2010	ASS-Low alloy steel	In dissimilar RSWs of low carbon steel and ASS, microstructure and hardness of the fusion zone which are controlled by dilution and fusion zone

				size of low carbon steel side mainly govern the failure mode
[8]	Pavethan R <i>et al.</i>	2011	Medium carbon steel-ASS	1 The formation of intermetallics such as Cr ₂₃ C ₆ and Cr ₇ C ₃ at the weld interface are responsible for higher hardness and lower tensile, impact and fatigue strength of the friction welded MCS-ASS dissimilar joints. 2 Fatigue strength of friction welded dissimilar joints of medium carbon steel and austenitic stainless is lower compared to the base metals.
[36]	Samal M K <i>et al.</i>	2011	ASS-ferritic stainless steel	The fracture resistance value of the joint with the crack located at the buttering-weld interface is the lowest because of the presence of the heat affected region at the edge of the welding region.
[9]	Cao J <i>et al.</i>	2012	ASS-martensitic stainless steel	1 The weak toughness of weld metal is attributed to its coarse dendritic austenitic structure. 2, The part of the joints with relatively weak tensile strength was T92 CGHAZ, while the part of the joints which revealed relatively weak toughness was weld metal.

2.4 Fatigue in metallic materials

Majority of engineering failures are caused due to fatigue. Study of fatigue properties in engineering structures is an area of interest for many scientist and researchers from the last century itself due to its catastrophic nature [37]. This section includes a brief overview of basic terminology, theories and various aspects of fatigue failures.

2.4.1. Cyclic loading in materials

Materials' behaviour under different loading conditions especially when it is subjected to continuously repeating loading-unloading cycles is always an important factor for design consideration. Various loading conditions may consist of stress levels starting from well below yield strength of material and goes up to ultimate tensile strength of material. The process of failure under these conditions is known as fatigue failures. Fatigue failures always occur at stress levels significantly lower than their monotonic fracture strength values [2][38]. In the present scenario, the basic understanding of metal fatigue holds a high relevance especially in the areas of automotive, aerospace, nuclear or hydrothermal power plants etc.; where parts like aircraft engines, turbines, rotors and compressors are

continuously subjected to vibration and fluctuating stresses. Fatigue failure may be catastrophic in nature but process of failure is progressive and consists of several stages. These stages and underlying failure mechanisms along with nomenclature and types of cyclic loading are discussed in section 2.4.1.1. Section 2.4.1.2 includes a brief discussion over major classification of fatigue on the basis of fatigue life of material like low cycle fatigue, high cycle fatigue and ratcheting.

Apart from repeated loads several other factors like temperature, environmental factors, geometry, sudden overloading, microstructure of material, residual stresses, and stress concentration may significantly influence the life of the material. These factors are discussed in more detail in section 2.4.1.3.

2.4.1.1. Mechanism of fatigue failure

The fatigue crack initiation process generally starts from free surface due to higher stresses and probable presence of defects like scratches, corrosive pits etc. It is also observed that fatigue cracks initiate even at highly polished defect free surfaces. The process of fatigue failure initiates with the formation of mature cracks that may grow during component's service life. Various microscopic changes that lead to change in crystalline structure of metals may occur under these conditions. These small scale changes increase the formation of small cracks. These small cracks further develop into larger cracks which grow continuously till the stresses become unsustainable and then catastrophic failure occurs. The process of fatigue failure can therefore be sub divided into three major stages (a) initiation of numerous small fatigue cracks, (b) growth of smaller number of small cracks into the larger ones and (c) final failure which is caused by a single through crack which propagates through the complete cross section of the components[37].

The formation of the cracks can be well described by following W A Wood's mechanism according to which the cracks originate due to repeated micro plastic deformations which result in the formation of "intrusion" and "extrusion" on specimen surface. These intrusions can act as notches which incorporate local stress concentration sites and favor formation of micro cracks. Formation of cracks and their initiation can be further divided into two steps as represented in Figure 2.2. (a) Crack grows initially in crystallographic manner and later on (b) in stage two when striation formation begins.

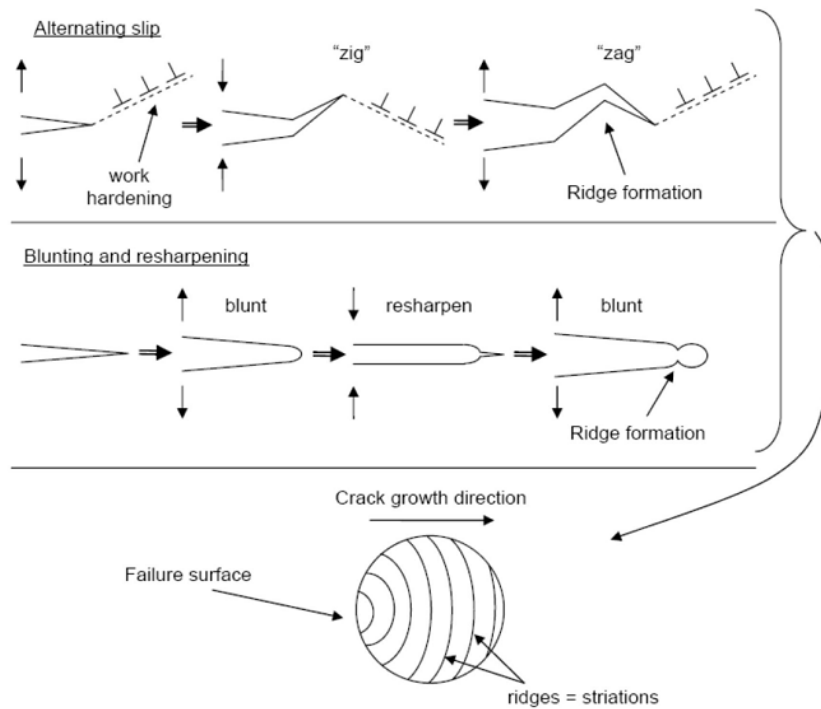


Figure 2. 2 Schematic representation of striation formation during fatigue crack growth [2,38].

Propagation of fatigue crack occurs through repeated crack tip blunting and sharpening effects. After a prolonged period of time this micro-plastic deformation mechanisms operating at the crack tip may cause characteristic markings which are called “beach markings” or “clamshell markings”. These markings are macroscopic in nature and can be visualized through a naked eye. On the other hand, there are extremely fine parallel markings, at intervals of the order of $0.1 \mu\text{m}$ called “striations”, which represent the crack growth or crack front due to each individual loading cycles and can see at higher magnifications using electron microscopes.

It has been observed that limited number of alternative slip planes occurred during crack tip plasticity. The resultant movement of dislocations is also limited to certain number of planes. Increasing number of dislocations near the crack tip cause pile up and result in localized work hardening. Resultant work hardening eases crack growth on slip plane by embrittling the material. Fig. 2.3 represents the various stages of fatigue crack growth. Further growth of crack activates new slip planes and the process repeats itself. The formation of zigzag paths and sharp ridges on failure surface by propagating crack can be attributed to the alternating

slip planes. Upon loading, the initially sharp crack will blunt due to plastic deformation and thus the lengths of small cracks increase due to blunting.

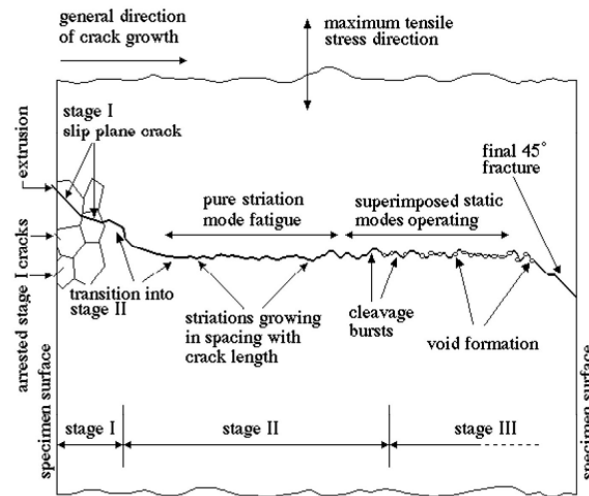


Figure 2. 3 Schematic representations of the various stages of fatigue crack growth [2]

When the crack is unloaded, the elastic stress field around the plastically relaxed crack tip will cause the crack to resharpen. The further reloading of the crack, blunting is again, leave a ripple on the surface. Further on, in Stage III, static fracture modes are superimposed on the growth mechanism, till finally it fails catastrophically by shear at an angle to the direction of growth.

Different nomenclature to describe test parameters

Different nomenclature is there in fatigue literature which can be enlisted as follows:

- **Stress range** ($\Delta\sigma$) = $\sigma_{\max} - \sigma_{\min}$
- **Stress amplitude** (σ_a) = $(\sigma_{\max} - \sigma_{\min}) / 2$
- **Mean Stress** (σ_m) = $(\sigma_{\max} + \sigma_{\min}) / 2$
- **Stress ratio** (**R**) = $\sigma_{\min} / \sigma_{\max}$
- **Amplitude ratio** (**A**) = $\sigma_a / \sigma_m = (1 - R) / (1 + R)$

2.4.1.2. Types of cyclic loading

As can be seen from Fig 2.4, cyclic loading may be of different types. These are: [Dieter 1998] completely reversed cycle: In this type of cyclic loading, maximum and minimum stresses are equal. It can also be referred as symmetric loading ($\sigma_m = 0$). Tensile stress is considered positive and compressive stress is negative (Fig 2.4(a)).

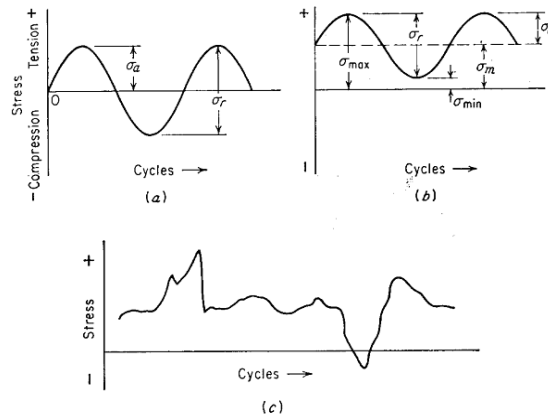


Figure 2. 4 (a) completely reversed stress cycle (b) asymmetric stress cycle (c) Random stress cycle.[37]

Asymmetric loading: repeated stress cycle in which the maximum stress σ_{max} and σ_{min} are not equal. Both are in tension, but sometimes it may be tension and compression both. This is known as asymmetric loading ($\sigma_m \neq 0$, Fig 2.4(b)). Random stress cycle: this type of stress cycle generated in a part such as an aircraft wing which is subjected to periodic unpredictable load due to gusts (Fig 2.4(c))[37].

2.4.1.3. Factors affecting fatigue life

Various parameters which play significant role in materials' fatigue life are enlisted in Table 2.3

Table2. 3 Factors affecting fatigue life

S.No.	Parameter	Role and Key Features
1	Microstructure	In general at ambient temperature, grain size is inversely proportional to fatigue life. Precipitate, grain boundaries, dislocation substructure and density along with phase transformation also influences fatigue

		life.
2	Processing type	Rolling, forging extrusion etc. produces directional properties. Fatigue life increases in longitudinal direction and decreases in transverse direction. Other processes like Heat treatment, case hardening induces residual stresses. Compressive residual stresses increases while tensile residual stresses decreases fatigue life.
3	Type of loading	Multiaxial loading reduces fatigue life more rapidly than uniaxial loading except pure torsional case. Alternating stress/strain has inverse relation with fatigue life.
4	Environmental condition	Corrosive atmosphere can have a detrimental effect on fatigue life.
5	Geometrical factors	Rough surfaces, notches, scratches, holes, joints decreases fatigue life by increases stress concentration.
6	Temperature	High temperatures $T > 0.5T_m$ fatigue life of material decreases. Grain boundary triple points increases resulting high stress concentration with increasing no. of grain boundary voids and wedge cracks.

2.4.2. Materials response to cyclic deformation

Any material when subjected to cyclic loading its deformation behaviour varies according to the various applied stress/strain parameters which are described in subsequent sections.

2.4.2.1 Bauschinger effect (Stress strain anisotropy)

According to a standard definition, the Bauschinger effect is the phenomenon by which plastic deformation increases yield strength in the direction of plastic flow and decreases it in other direction” [39]. The Bauschinger effect is schematically described in Fig 2.5 by using an idealized material under uniaxial loading. Mechanism of Bauschinger effect can be put forward using three model theories. First one “internal stress theory” states the non-uniformity of stresses during plastic deformation. These non-uniform stresses result in residual stresses which lowers the yield upon load reversal. Second “composite model theory” emphasizes materials behaviour as composite consisting of two phases on load reversal. Residual stresses in softer field causes premature yield[39].

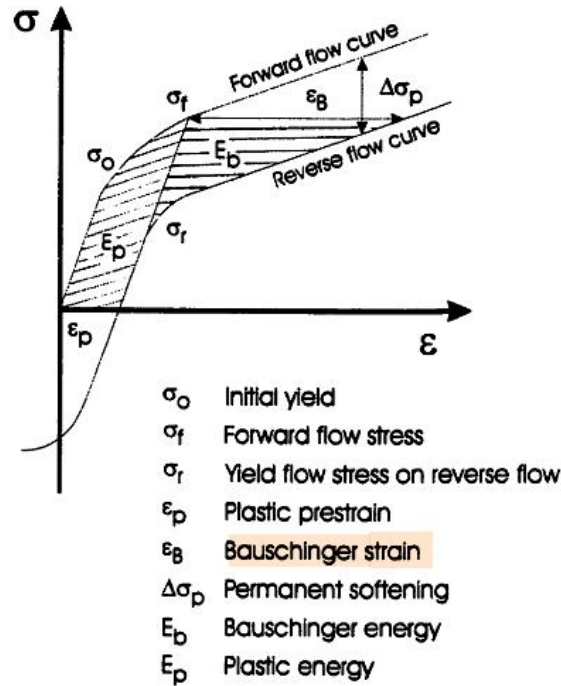


Figure 2. 5 Schematic representation of Bauschinger effect [39]

Finally “dislocation theory” which put forward the role of grain boundaries as barrier to dislocation motion. As a result, the back stresses produced by dislocation piled up and assist motion in the reverse direction by lowering yield. [39].

2.4.2.2 Hardening softening behaviour

Cyclic hardening/softening refers to response of a material subjected to repeated loading. In most of the cases under fully reversed strain-controlled loading with controlled strain amplitude, a material is cited to display cyclic hardening/softening when the stress amplitude increases/decreases.

Certain materials, such as the stainless steels and pure copper, annealed steel, exhibit very significant cyclic hardening while some other materials display less significant hardening or softening [40]. In simple words hard material cyclically softens and a soft material cyclically hardens. Schematic diagrams are illustrated in Fig 2.6 for cyclic hardening and softening materials respectively. Many engineering materials usually exhibit cyclic hardening/softening to some extent in cyclic plastic deformation process.

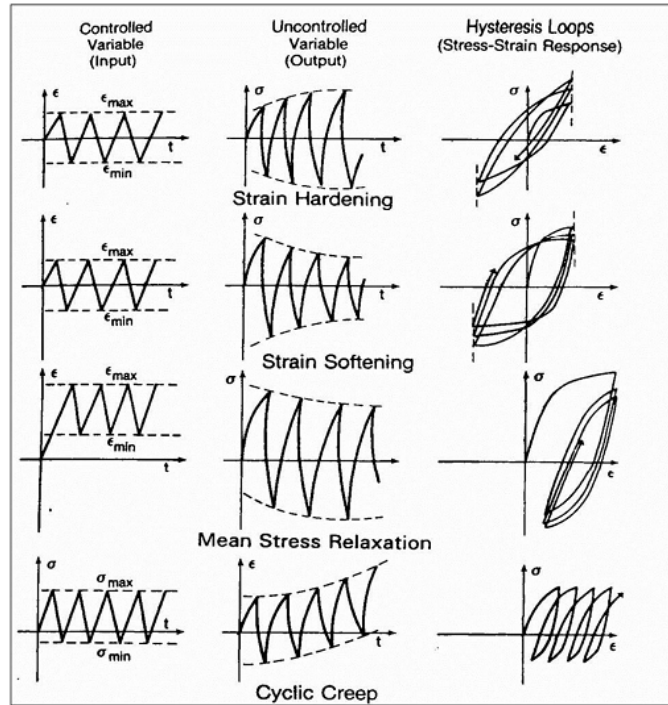


Figure 2.6 Schematic response to various cyclic input variables [37]

In general practice, the details about cyclic hardening/softening from a large number of published literatures is more or less qualitative in nature. However Shang 1996 and Ye Duyi 2006 [41][42], introduced the concept of cyclic hardening factor (or softening factor); with this single factor cyclic hardening of both strain and stress controlled fatigue cannot be represented. For strain controlled fatigue it is the ratio of stress amplitude at any cycle to stress amplitude at first cycle, For strain controlled experiments hardening factor (H_e) [41] can be expressed as

$$H_e = \frac{\Delta\sigma_s - \Delta\sigma_1}{\Delta\sigma_1}$$

where, $\Delta\sigma_s$ = stress amplitude at saturated cycle and $\Delta\sigma_1$ = stress amplitude at first cycle

$H_e, H_s > 0$ for cyclic hardening materials

$H_e, H_s < 0$ for cyclic softening materials

Another approach for quantitative measurement of hardening/softening is loop shape parameter (LSP), V_H . The evolution of this parameter throughout the cyclic loading test indicates the occurrence of persistent slip bands at the surface of the specimen [43]. The V_H parameter is given by the following equation

$$V_H = \frac{W}{4\varepsilon_{ap}\sigma_a}$$

Where, W is the hysteresis loop area, ε_{ap} is the plastic strain amplitude and σ_a is the stress amplitude. During initial cyclic hardening and the development of the vein dislocation structure, V_H decreases. However, localization of plastic strain in persistent slip bands (PSB's) is accompanied by a significant increase in V_H . This increase is especially pronounced in single crystals, though it has also been observed in polycrystals [44]. After the stress amplitude of the specimen cyclically saturates, V_H either reaches a plateau or decreases slightly.

2.4.2.3. Mean stress relaxation

Relaxation of mean stress happens when we do an unsymmetrical strain experiment, as shown in Fig 2.6. For unsymmetrical strain experiment, a mean strain is introduced. Mean strain cause mean stress. So at the initial cycle a mean stress is introduced during unsymmetrical strain experiment. But as the cycling proceeds mean stress will relax and tends to zero.

2.4.2.4. Ratcheting

Ratcheting is the event of progressive accumulation of permanent deformation when any component is subjected to cyclic loads in the elastic plastic strain range under stress controlled fatigue with non-zero mean stresses. Due to accumulation of plastic strain material will finally lead to a shakedown, or a constant rate of ratcheting or very large ratcheting strains ultimate to failure of the material [45]. Ratcheting is important in designing and life evaluation of the structural components endured in cyclic loading. Ratcheting strain is a secondary strain produced under asymmetrical cyclic stressing, and has a great dependence on loading conditions and loading history

2.4.3 Loop analysis

2.4.3.1 Cyclic stress strain curve (CSSC)

As is shown in Fig. 2.7, the stress range, $\Delta\sigma = \sigma_{max} - \sigma_{min}$ and the strain range can be analogously be represented as. $\Delta\varepsilon = \varepsilon_{max} - \varepsilon_{min}$. The corresponding amplitudes of stress and strain are half the ranges. The plastic strain range $\Delta\varepsilon_{pl}$ is equal to

the distance between the points of intersection of the hysteresis loop and the strain axis, as is shown in Fig. 2.8. Depending on the material, a more-or-less pronounced back deformation may occur during unloading, which gives rise to a difference between $\Delta\varepsilon_p$ and $|\varepsilon_{max} - \varepsilon_{min}|$. This difference sometimes attributed to a “reversible plastic strain,” an expression that itself seems contradictory. When constructing a strain-time history from stress-time data hysteresis loop have to be constructed using the cyclic stress-strain curve (CSSC). One key step is to determine when the line begins to bend as we move from tension to compression and vice versa. This is handled by using Masing’s hypothesis, which assumes that the line describing a stress-strain hysteresis loop is geometrically similar to the CSSC but numerically twice its size[2]. Consequently, the equation of the curve can be directly derived from the equation of CSSC. In order to distinguish the parameters representing monotonic and cyclic ones, a prime symbol is used for cyclic parameters. Corresponding to any point (σ, ε) on CSSC, we have,

$$\varepsilon = \varepsilon_e + \varepsilon_p = \frac{\sigma}{E} + \left(\frac{\sigma}{K'}\right)^{\frac{1}{n'}}$$

Where, K' is called the cyclic strength coefficient and n' is called the cyclic strain hardening exponent. From Masing’s hypothesis, the same point can be located on the hysteresis loop curve and it will have coordinates $(\Delta\sigma, \Delta\varepsilon)$ where:

$$\Delta\varepsilon = 2\varepsilon \text{ and } \Delta\sigma = 2\sigma$$

Substituting into the equation for CSSC, we have

$$\frac{\Delta\varepsilon}{2} = \frac{\Delta\varepsilon_e}{2} + \frac{\Delta\varepsilon_p}{2} = \frac{\Delta\sigma}{2E} + \left(\frac{\Delta\sigma}{2K'}\right)^{\frac{1}{n'}}$$

Which in general case reduces to

$$\Delta\varepsilon = \frac{\Delta\sigma}{E} + 2\left(\frac{\Delta\sigma}{2K'}\right)^{\frac{1}{n'}}$$

Thus we can establish the relationship between the cyclic stress-strain curve and hysteresis loop shape. Proceeding on the similar grounds, we have

$$\frac{\Delta\sigma}{2} = K' \left(\frac{\Delta\varepsilon_p}{2}\right)^{n'}$$

$$\frac{\Delta \varepsilon_p}{2} = \frac{\Delta \varepsilon}{2} - \frac{\Delta \sigma}{2E}$$

The cyclic stress-strain curve reflects the resistance of a material to cyclic deformation and can be different from monotonic stress-strain curve.

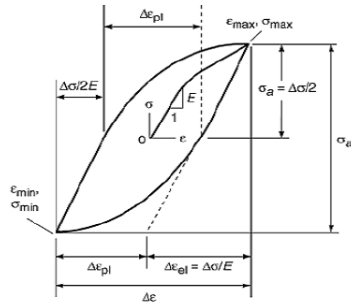


Figure 2. 7 Primary quantities of a hysteresis loop. [2]

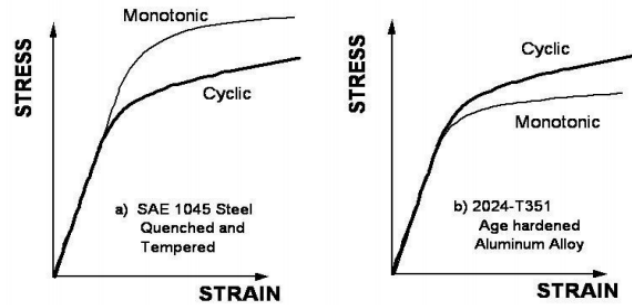


Figure 2. 8 Comparison of CSSC and MSSC curve illustrating cyclic hardening and cyclic softening respectively [57].

Transient cyclic deformation behavior such as cyclic hardening or cyclic softening refers to a continuous change in the cyclic strength that may occur throughout a test or at least in the first stage of cyclic deformation. Schematic examples of cyclic hardening and cyclic softening in are shown in Fig. 2.9 show the stress change and hysteresis loop shape. Cyclic hardening leads to an increase in the stress amplitude, and consequently the hysteresis loop becomes larger. Cyclic softening has the opposite effect a decrease of and a reduction of the size of the $\frac{\Delta \sigma}{2}$ hysteresis loop. The type of transient behavior is mainly determined by the pretreatment of the material tested. It is plausible that, for instance, heavy cold working prior to cyclic loading could cause subsequent cyclic softening, whereas a recrystallization treatment could give rise to cyclic hardening. Furthermore, deformation induced micro-structural changes may also be the reason for transient deformation behavior.[37]

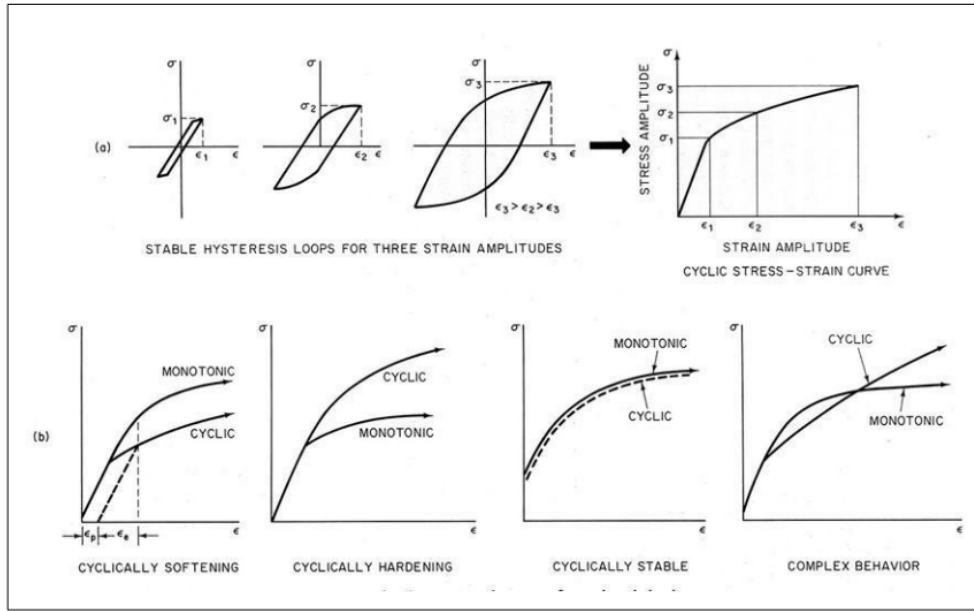


Figure 2. 9 Schematic representation of transient cyclic deformation processes [57].

2.4.3.2. Masing vs. non Masing behavior

As discussed earlier, Masing described the cyclic stress strain behaviour of polycrystals in a model [2], where it was assumed that a number of elementary volumes can be considered to represent grains of different orientations and the deformation behaviour of each element was considered to be ideally elastic plastic. The model also attributed each such element individual yield strength and it was assumed that similar elements (same orientation) are strained in parallel. The distribution of the elements was chosen in such a way as to represent the actual variations in local yield stress within the microstructure. An implicit assumption in Masing's consideration is that a microstructural change does not occur during loading, which means the same microstructure and deformation mechanisms prevail at all plastic strain amplitudes applied. So it can be implied that the stress-strain path after load reversal would follow a unique curve regardless of the amplitude of loading. When a material exhibits this kind of behaviour, it is said to be a Masing material. Any deviation from this behaviour characterizes the material as non-Masing material. For this purpose the compressive tips of the stable hysteresis loops of different strain amplitudes are brought to a common origin by translation method and checked if they form a common envelope curve or not[46]. Fig.2.10 (a) and 2.10 (b) represent Masing behaviour (form a common envelope) and non-Masing behaviour (does not form

a common envelope) of the material. However, the extent of deviation from Masing behaviour varies with strain amplitudes.

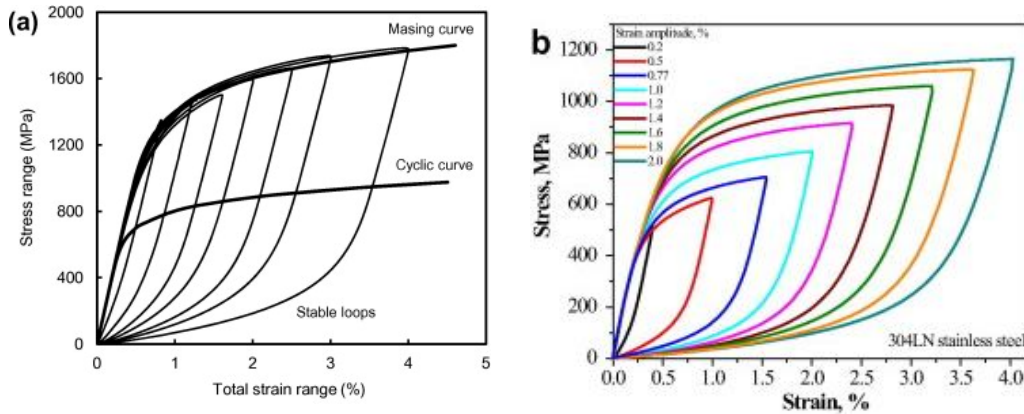


Figure 2. 10 Schematic representation of (a) Masing behaviour (b) non Masing behaviour [46, 40].

2.4.3.3 Master curve

From the engineering point of view, a mathematical description of the branches of the hysteresis loop is required so that properties such as hysteretic energy (plastic strain energy) and proportionality limit can be calculated with strain range variation to measure the extent of deviation from Masing behaviour. Master curves are constructed by matching the loading branches of stable hysteresis loops of different strain ranges, by translating each loop along the linear elastic portions. By translating the loops along the elastic slope from the origin, it was possible to accurately match all the upper branches, as shown in Fig.2.11. The lower tips lay along the linear elastic line. The common envelope curve with respect to the new origin translated to the compressive tip of the smallest strain range hysteresis loop forms the master curve. The equation for the master curve corresponding to the hysteresis loop with minimum strain range (i.e., with respect to the translated axis) can be written as [2]

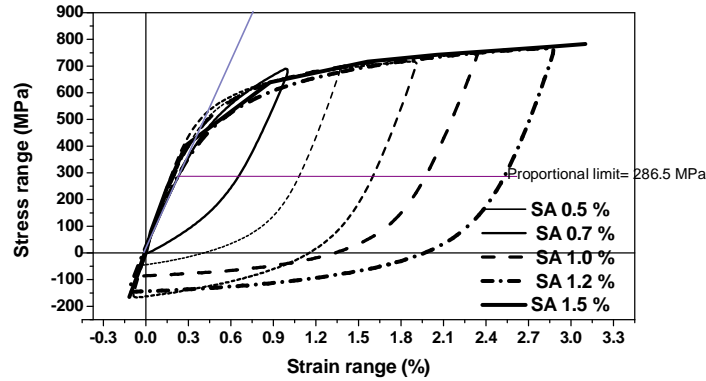


Figure 2. 11 Typical master curve [2]

$$\Delta \varepsilon^* = \frac{\Delta \sigma^*}{E} + 2 \left(\frac{\Delta \sigma^*}{2K^*} \right)^{1/n^*}$$

Where asterisk superscript indicates that the quantity is measured with respect to the translated co-ordinate system. The values of K^* and n^* are found by fitting above equation to the experimental data.

2.4.3.4 Plastic strain energy

During cyclic loading, energy is dissipated because of plastic deformation. The plastic strain energy, ΔW_p , absorbed in a cycle is the area of the hysteresis loop, i.e., the area enclosed under the cyclic stress versus cyclic strain in a closed loop per cycle as shown in Fig 2.12. For a Masing material, this is given by:

$$\Delta W^p = \frac{1-n}{1+n} \Delta \sigma \Delta \varepsilon^p$$

where $\Delta \varepsilon_p$ is the plastic strain range, $\Delta \sigma$ is the stress range, and n is the cyclic strain hardening exponent. If $\delta \sigma_0$ denotes the proportional stress limit [4], then the plastic strain energy for a Masing material is given as:

$$\Delta W_M^p = \frac{1-n^*}{1+n^*} \Delta \sigma^* \Delta \varepsilon^* = \frac{1-n^*}{1+n^*} (\Delta \sigma - \delta \sigma_0) \Delta \varepsilon^p$$

where n^* is the strain hardening exponent of the master curve. Following similar grounds, the plastic strain energy of the hysteresis loop for a material exhibiting non Masing behaviour is given by:

$$\Delta W^p = \frac{1 - n^*}{1 + n^*} (\Delta\sigma - \delta\sigma_0) \Delta\varepsilon^p + \delta\sigma_0 \Delta\varepsilon^p$$

Above equation can be rewritten in the following form as:

$$\Delta W_M^p = \frac{1 - n^*}{1 + n^*} \Delta\varepsilon^p \Delta\sigma + \frac{2n^*}{1 + n^*} \delta\sigma_0 \Delta\varepsilon^p$$

The increase in the proportional stress limit $\delta\sigma_0$, which describes the cyclic hardening or softening, can be easily obtained when the cyclic and master curve equation are known.

$$\delta\sigma_0 = \Delta\sigma - \Delta\sigma^* = \Delta\sigma - 2K \left(\frac{\Delta\varepsilon^p}{2} \right)^{n^*}$$

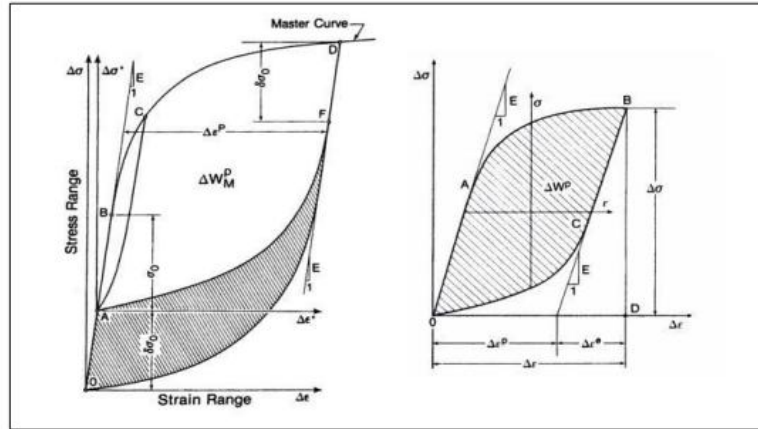


Figure 2. 12 Plastic strain energy calculation (a) Masing material (right) (b) Non Masing material (left) [2].

2.4.4. Different approaches for predicting fatigue life

Fatigue life prediction through various approaches is discussed in this section.

2.4.4.1. Stress based approach

This approach is suitable when the applied stress is nominally within the elastic range of the material and the number of cycles to failure is large. Hence, this approach is best suited to the problems that fall into the category known as high-cycle fatigue (HCF).

In HCF, the life is usually characterized as a function of the stress range applied, and the components fail after large numbers (Usually higher than 10^6 cycles) of cycles at a relatively low stress (Usually less than 30% of yield stress), and the deformation experienced is primarily elastic. High cycle fatigue must be considered during design of

automobiles, aircrafts, compressors, pumps, turbines, etc where vibration occur. HCF test is done at frequency always greater than 1 KHz. The stress-cycles to failure in high cycle region is sometimes described by the Basquin equation as shown in Fig. 2.13.

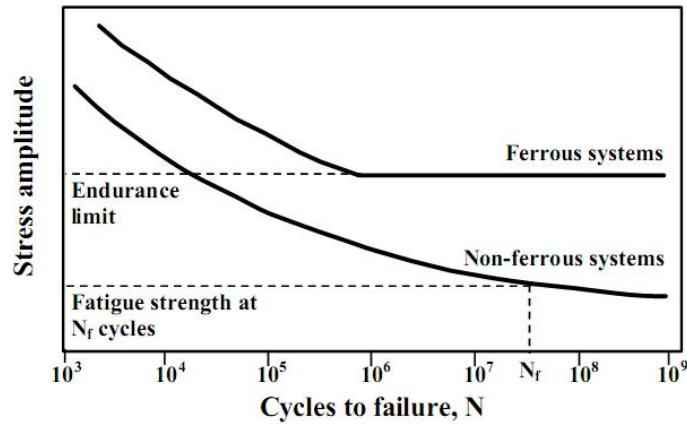


Figure 2. 73 Schematic representation of S N curve [37]

and is given by a established power law description of fatigue life:

$$\sigma_a = \sigma_f (N_f)^b$$

Where σ_f is the fatigue strength coefficient and b is the fatigue strength exponent, these parameters are the fatigue properties of materials. Fatigue strength coefficient is equal to fracture stress at the time of monotonic tension. Fatigue strength exponent b varies from 0.05 to -0.15 for most metals [2] b is also related to cyclic strain hardening exponent as follows

$$b = \frac{-n'}{1+5n'}$$

The mean stress effect can be accounted, then Basquin relation takes the following shape:

$$\sigma_a = (\sigma_f - \sigma_m)(N_f)^b$$

Where, σ_m is the mean stress.

2.4.4.2. Strain based approach

This approach was introduced, initially, for thermal and low cycle fatigue. Here life is nominally characterized as a function of the strain range and the component fails after a small number of cycles at a high stress, and the deformation is largely plastic. Strain controlled cyclic loading is found in thermal cycling, where component expands and

contracts in response to fluctuations in the operating temperature. Low cycle fatigue must be considered during design of nuclear pressure vessels, steam turbines and other types of power machineries. Low cycle fatigue test is done at frequency less than 1 Hz. The usual way of presenting low-cycle fatigue test results is to plot the plastic strain range $\Delta\varepsilon_p$ against N_f . The behaviour of low cycle fatigue is described by Coffin-Manson relation, represented in Fig 2.14

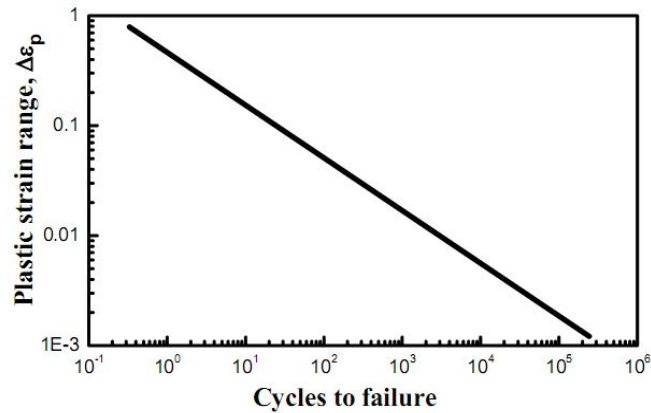


Figure 2. 14 Schematic representation of Coffin Manson plot.[37]

$$\Delta\varepsilon_p/2 = \varepsilon'_f(2N)^c$$

Where, $\Delta\varepsilon_p/2$ = plastic strain amplitude

ε'_f = fatigue ductility coefficient defined by strain intercept at $2N = 1$

$2N$ = number of strain reversals to failure

c = fatigue ductility exponent, which varies between -0.5 to -0.7 for many metals.

ε'_f correlates very well with the true strain to fracture in a monotonic test, and c varies between approximately -0.5 and -0.7 for most metals [[2]]. The fatigue ductility exponent can also be computed from this relation

$$c = \frac{-1}{1 + 5n'}$$

2.4.4.3. Energy based approach

On the microscopic level, the irreversible nature of micro plastic deformation caused by each cycle of loading is associated with the dissipation of strain energy density. The dissipation strain energy density per cycle may be regarded as a contributor to the fatigue damage process per cycle. This approach can be broadly classified into two sub-categories as follows: 1. Hysterisis based approach 2. Total energy approach

Hysterisis based approach: discussed earlier

Total strain energy approach:

The area enclosed in the cyclic stress-strain loop is representative of the hysteresis energy. This is represented in Fig 2.15. A major part of it is dissipated into heat and vibration and the remaining part causes damage in the form of slip along crystallographic planes and movement of the dislocations [2]. As is evident, the total strain energy is the sum of hysteresis energy and elastic energy, and is given as:

$$\Delta W^t = \Delta W^e + \Delta W^p$$

The elastic strain energy density, per cycle is computed as follows:

$$\Delta W^e = \frac{1}{2E} \left(\frac{\Delta\sigma}{2} + \sigma_m \right)^2 = \frac{\sigma_{max}^2}{2E}$$

Coupling above two equations get

$$\Delta W^t = \frac{1 - n^*}{1 + n^*} \Delta\varepsilon^p \Delta\sigma + \frac{2n^*}{1 + n^*} \delta\sigma_0 \Delta\varepsilon^p + \frac{\sigma_{max}^2}{2E}.$$

Using equations Basquin, Coffin Manson and Proportional limit equation, we can write

$$\Delta W^t = k_t (2N_f)^{\alpha_t} + \Delta W_0^t$$

where $k_t > 0$ and $\alpha_t < 0$. When $2N_t \rightarrow \alpha$, $\Delta W^t \rightarrow \Delta W_0^t$, thus

$$\Delta W_0^t \approx \left(\frac{\sigma_{max}^2}{2E} \right)_{fatigue\ limit}$$

The constant is the elastic strain energy of the material fatigue (endurance) limit. The other two material constants, k_t and α_t , may be determined from the best fit to experimental data.

$$\frac{\Delta W^t - \Delta W_0^t}{k_t} = (2N_f)^{\alpha_t}$$

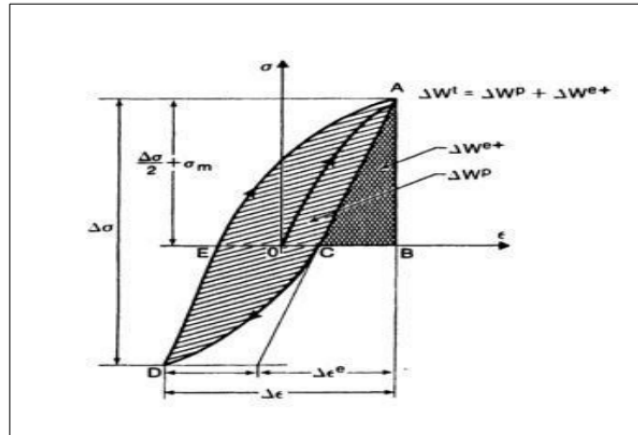


Figure 2.15 Total strain energy approach [2]

2.4.5 Fatigue life estimation models

In the design and development of engineering components fatigue life predictions takes important role. Various methods that can be used for predicting fatigue life are .Basquin, Coffin Mansion, Smith Watson Topper (SWT) and Walker equation etc. Basquin's equation and Coffin Mansion equation are already discussed in earlier sections so remaining methods (SWT and Walker) are discussed in this section.

2.4.5.1. Walker parameter

Walker proposed [3] a model in which quantity γ is a fitting constant that may be considered to be a materials property.

$$\sigma_{eq}^{walker} = \sigma_{max}^{1-\gamma} \sigma_{amp}^{\gamma}$$

$$\sigma_{eq}^{walker} = \sigma_{max} \left(\frac{1-R}{2} \right)^{\gamma}$$

Walker equation

$$\log_{10} N_f = \frac{1}{b} \log_{10} \sigma_{max} + \frac{\gamma}{b} \log_{10} \left(\frac{1-R}{2} \right) - \frac{1}{b} \log_{10} \sigma_f - \frac{1}{b} \log_{10} 2$$

2.4.5.2. SWT lifing equation

Smith, Watson, and Topper [3] proposed a method that assumes that the amount of fatigue damage in a cycle is determined by $\sigma_{max} \epsilon_a$, where σ_{max} is the maximum tensile stress and ϵ_a the strain amplitude. Also, SWT parameter is simply a statement that $\sigma_a \epsilon_a$, for a fully reversed test is equal to $\sigma_{max} \epsilon_a$, for a mean stress test."

$$\sigma_a^{eq} = \sqrt{\sigma_a \sigma_{max}} = \sigma_a \sqrt{1 + \frac{\sigma_m}{\sigma_a}} = \sigma'_f (N_f)^b$$

Where σ_{max} is the maximum stress in a hysteresis loop.

2.5 Summary

The present chapter summarizes the published work of earlier researchers related to mechanical behavior of DMW and brief overview of the cyclic deformation behavior of materials. Although much work has been done in this regard but the lack of systematic study of weld zone in DMW joints which can examine the material with the help of various fatigue approaches forms the basis of present investigation.

The present study aims to investigate the low cycle fatigue behavior of AISI 308 SS weld metal with help of strain based and energy based approaches. Fatigue life prediction through various models (SWT and Walker) also been performed to quantify fatigue life of the material.

Chapter 3

3.0 Materials and methods

3.1 Introduction

3.2 Experimentation

3.2.1 Material

3.2.2 Chemical composition

3.2.3 Optical microscopy

3.2.4 Hardness measurement

3.2.5 Tensile test

3.2.6 Low cycle fatigue

3.2.7 Scanning electron microscopy

Chapter 3

Materials and Methods

3.1 Introduction

A brief introduction to the weld metal (material under investigation), the dimensional details of the low cycle fatigue specimen and basic material characterizations are described in this chapter. The study of low cycle fatigue is the objective of present investigation. The details of the low cycle fatigue test procedures are also presented in the chapter.

3.2 Experimentation

3.2.1 Materials

The dissimilar welded stainless steel pipes were received in as welded condition from Bhabha Atomic Research Center, Mumbai, India. Following are the dimensional details of the as received material (in the form of DMW pipe):

Outer diameter: 325 mm and Wall thickness: 25 mm.

Weld zone of SS308 is cut through the supplied welded pipes after precise identification of weld zone as shown in Fig. 3.1.

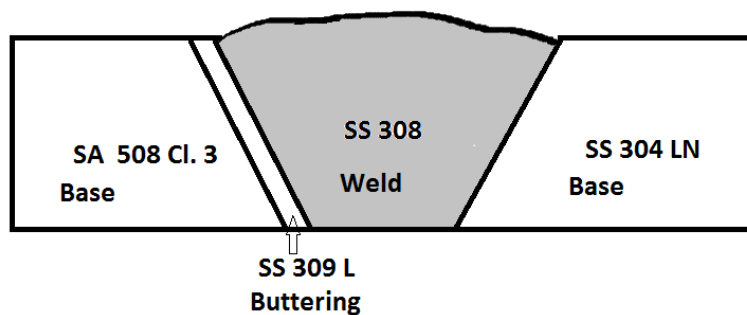


Figure 3. 1 Schematic representation of welded block

3.2.2 Chemical composition

The chemical composition of the weld metal materials was examined using spark optical emission spectrometer (model: Q6 columbus, Bruker corporation limited, USA).

3.2.3 Microscopic examinations and image analysis

Metallographic specimens of approximately 10 mm × 10 mm cross-section or of 10 mm diameter with 8-10 mm thickness were cut from weld zone of as-received pipes using a slow speed diamond cutter. The polished specimens were etched with Murakami's reagent (10 g KOH, 10 g K₃[Fe(CN)₆] and 100 ml H₂O). Microstructures of the specimens in all three LR, RC and LC orientations were examined under an optical microscope (Leica, model: DM 2500 M) and representative photographs were recorded. The microstructures were also image analysed with the help of Lieca image manager IM 50 software. The ferrite number was measured using Magne Gage as per recommendations of American welding society (AWS) for ferrite number 2-28. The volume fraction of different phases were measured (repeated over 50 random images) using Clemex Image Analyzer version PE 3.5.

3.2.4 Hardness measurement

Hardness values of weld SS308 were measured using Vickers hardness testing machine maintaining indentation load of 30 kgf and dwell time of 5 s (Leco Model, LV 700, MI USA). Minimum 5 readings were taken for each specimen to obtain the average value. Tests were performed as per ASTM standard E384[47]. The Vickers hardness was calculated using the expression:

$$H_v = \frac{1.854 \times P}{D_{avg}^2}$$

Where,

P = indentation load.

$D_{avg} = \frac{d_1 + d_2}{2}$, in which d₁ and d₂ are the lengths of two indentation diagonals.

3.2.5 Tensile test

Uniaxial tensile testing of weld zone was performed using flat tensile sub-size specimens fabricated as per ASTM E8M -2011[1]. Specimens were made from blank using a cut through pipe as shown in Fig. 3.2 (a) and (b). Specimens are made from pure weld zone,

as mentioned earlier in the thesis study has been carried out for pure weld zone further the nomenclature LR, LC, and RC represent Longitudinal-Radial (LR), Longitudinal-Circumferential (LC) and Radial-Circumferential (RC) respectively, and can be represented during the time of presentation. Furthermore, Fig 3.2 represent plan for specimen preparation while Fig 4.1 represents microstructure characterisation of different orientations. Dimensions of sub-size specimen are presented in Fig. 3.3. All tests were performed at strain rate of 10^{-3} /sec and data acquisition rate 5 Hz with the help of universal testing machine (Instron 8862) in ambient environment.

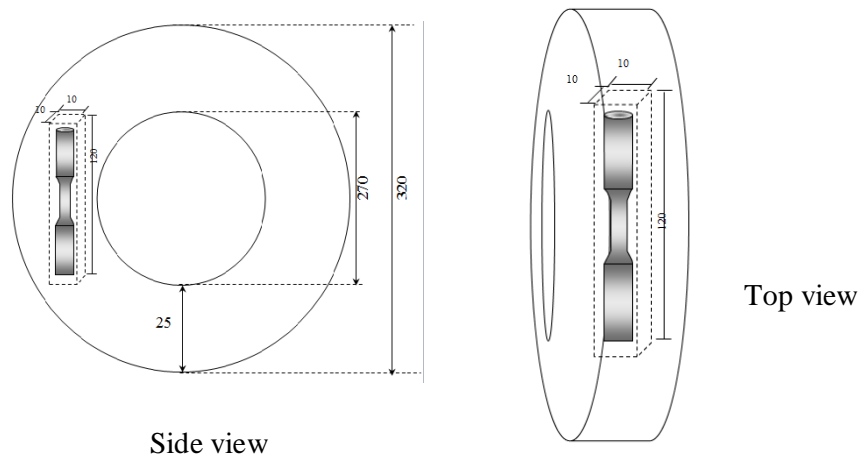


Figure 3. 2 Orientation and specimen preparation plan through pipe (a) Side view (b) Top view

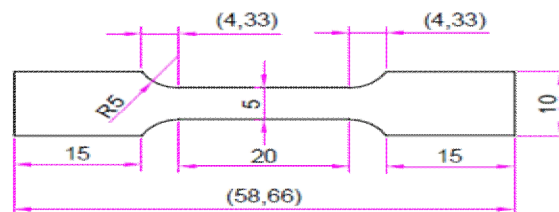


Figure 3. 3 Flat tensile subsize weld specimen. All dimensions are in ‘mm’

The measurements of strain during the tensile tests were made using an extensometer. At least three tensile tests were carried out to estimate the average tensile properties. The load-displacement data were recorded during the tests using the Wave Matrix software package.

3.2.6. Low cycle fatigue test

Specimen geometry

Flat tensile sub-size specimen of 8 mm gauge length and 5 mm thickness (as shown in Fig. 3.4) were fabricated from weld zone maintaining loading axis of the specimen parallel to the longitudinal dimension of the pipe.

All dimensions are in mm

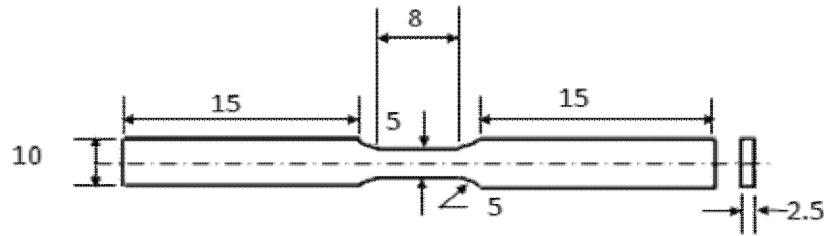


Figure 3. 4 Schematic diagram depicting flat sub size room temperature fatigue specimen

Test Methodology

All the low cycle fatigue experiments were carried out at room temperature using a 100kN servo-electric testing system (Instron-8862) supported by Wave Matrix software. The system was attached to a computer to control the tests as well as for data acquisition. All tests were conducted in strain control mode till fracture using triangular waveform as per ASTM E 606 [48](as shown in Fig. 3.5) at a constant strain rate of $10^{-3}s^{-1}$. The frequency and data acquisition rate are measured with the help of strain rate and strain amplitude. Resultant set of hysteresis loops are represented in (Fig. 3.6).

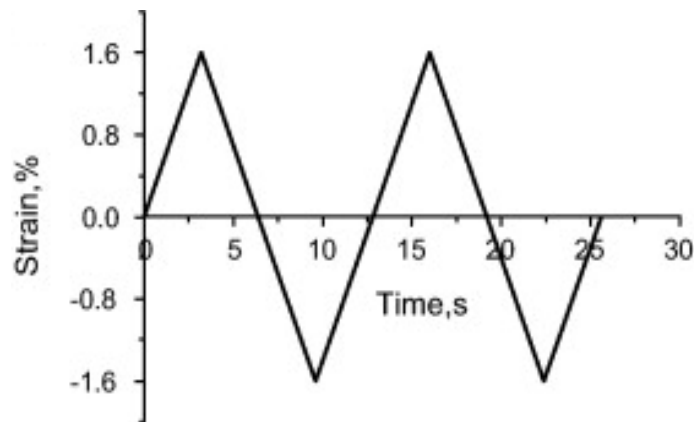


Figure 3. 5 Typical Wave form used for low cycle fatigue test. age | 36

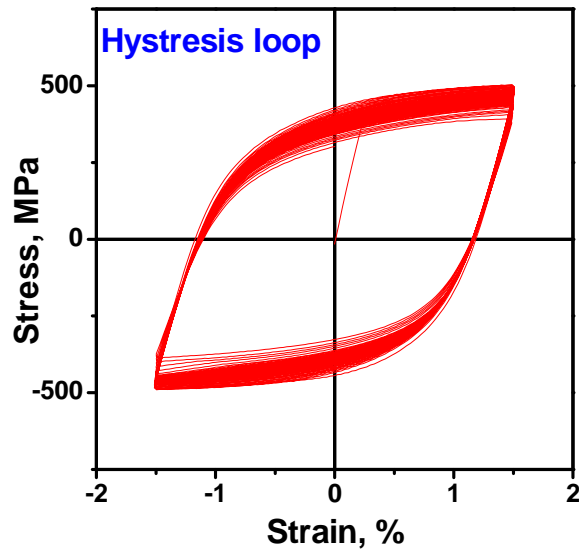


Figure 3. 6 Typical hysteresis loops as generated during experiment

The following parameters were maintained during LCF test:

Frequency = [strain rate / (4 x strain amplitude)] cycles/ s.

Data acquisition rate = Total data points per cycle x frequency

Strain amplitudes = $\pm 0.5\%$, $\pm 0.7\%$, $\pm 1.0\%$, $\pm 1.2\%$ and $\pm 1.5\%$

Each test was repeated for its conformity. Total 200 data points were collected during each cycle or stored hysteresis loop. Details of these tests are summarized in Table 3.1.

Table 3. 1 Summary of low cycle fatigue tests

Strain amplitude	N_f	Frequency (hertz)	(e_p) (%)
$\pm 0.5\%$	2534	0.0500	0.20631
$\pm 0.7\%$	1024	0.0357	0.4392
$\pm 1.0\%$	455	0.0250	0.71089
$\pm 1.2\%$	402	0.0208	0.89053
$\pm 1.5\%$	98	0.0167	1.1501

3.2.7 Fractography

Fracture surfaces of tensile and LCF specimens of various strain amplitudes were examined using Scanning Electron Microscope (FEG SEM Nova Nano SEM 430).

Chapter 4

4.0 RESULTS AND DISCUSSIONS

4.1 Introduction

4.2 Basic characterization of weld SS 308

4.2.1. Chemical composition

4.2.2. Microstructural evaluation

4.2.3. Hardness

4.3 Tensile test of the metal

4.3.1 Engineering stress strain behaviour

4.3.2 True stress strain behaviour

4.3.3. Fractographic analysis of fracture specimens

4.4 Cyclic deformation behaviour of weld SS 308

4.4.1. Bauschinger effect

4.4.2. Cyclic hardening softening behaviour

4.4.3 Variation of Loop shape parameter

4.4.4. Stability in cyclic stress and strain

4.4.5. Coffin Manson plot

4.4.6. Variation of total energy with strain amplitude

4.4.7. Cyclic stress strain curve

4.4.8. Comparison of MSSC and CSSC

4.4.9. Masing/ non Masing behaviour

4.4.10. Master curve

4.4.11 Variation of Plastic energy with strain amplitude

4.4.12 Fatigue life estimation

4.4.12.1. Walker model

4.4.12.2. Smith Watson Topper (SWT) model

4.4.13 Fractography of fatigue specimen

Chapter 4

Results and discussions

4.1 Introduction

The chemical composition, microstructural analysis and hardness of weld metal are reported in section 4.2. Tensile behaviour of the material are presented and discussed in section 4.3. The results of the LCF test are presented in section 4.4. The generated data are analysed and discussed for Bauschinger effect, hardening/ softening behaviour, Masing / non Masing character, plastic strain energy and fatigue life estimation models.

4.2 Basic characterization of material

4.2.1. Chemical composition

AISI 308 SS is an austenitic grade stainless steel containing 12-27% chromium, 7-25% nickel and very low amount of carbon. However, weld composition often depends on process parameters. The chemical composition of weld zone (SS 308) are presented in Table 4.1 (all in wt. %).

Table 4. 1 Chemical composition of the material

Material	Elements (wt. %)												
	C	Si	Mn	P	S	Cr	Mo	Ni	Co	Cu	V	N	Fe
Weld SS 308	0.026	0.456	1.045	0.026	0.011	20.797	0.085	9.463	0.046	0.247	0.065	0.073	Rest

4.2.2. Microstructural evaluation

Representative microstructures of weld metal in different orientations are presented in Fig 4.1. The microstructures exhibited the presence of dendrites of delta ferrite dispersed in austenitic matrix. Dendrite size of weld SS 308 were measured using Magne gage and the ferrite number was found in the range of 8-12. The volume fraction of different phases in weld SS 308 evaluated with the help of Clemex image analyser and the estimated values are reported in Table 4.2. Results show presence of nearly same amount of dendrite phase

in different orientations. It may be noted that the presence of 10-15 volume % of dendritic delta ferrite phase helps to avoid hot cracking of austenitic matrix at high temperatures [49].

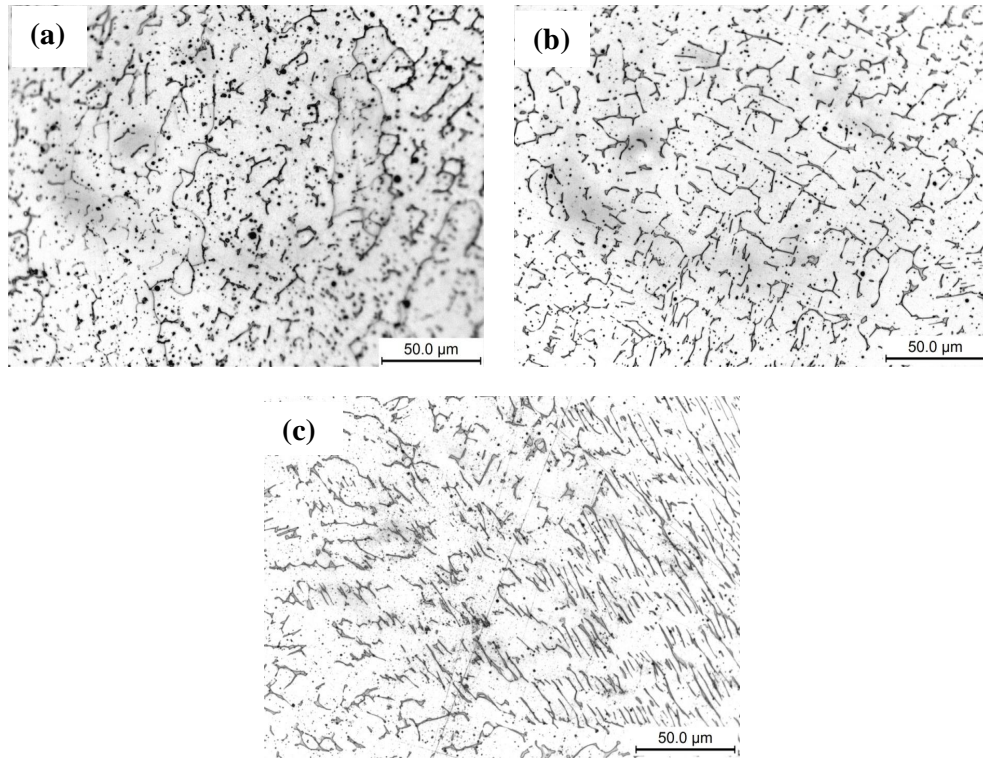


Figure 4. 1 Weld zone microstructure in different orientation (a) RC, (b) LC, (c) LR

Table 4. 2 Ferrite volume fraction in weld SS

	Vol fraction of Austenite	Vol fraction of Dendrites of δ Ferrite
Weld SS 308 (LC)	87.975	12.025
Weld SS 308 (CR)	84.97	15.03
Weld SS 308 (LR)	85.63	14.37

4.2.3. Hardness behaviour of material

The average Vickers hardness values in different orientations of weld zone is tabulated in Table 4.3. The higher value of hardness in RL orientation of weld zone may attribute to the variation in the microstructure.

Table 4. 3 Average hardness values in weld zone

Weld SS 308	RL	LC	RC
HV value	224	210	209

4.3 Tensile deformation behaviour of weld SS 308

4.3.1 Engineering stress strain behaviour of weld SS308

Tensile sub-size specimens were used to investigate tensile properties of the material. Fig 4.2 represents engineering stress strain curve of the material. The 0.2% offset yield strength (YS), ultimate tensile strength (UTS), percentage uniform elongation ($\% \epsilon_u$) and percentage total elongation ($\% \epsilon_t$) are tabulated in Table 4.4.

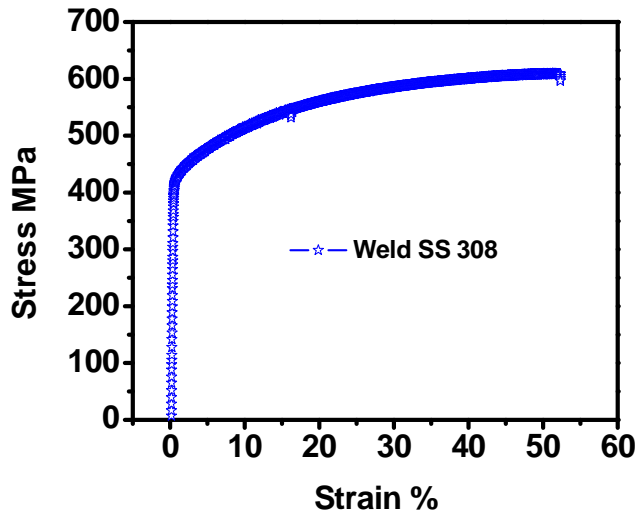


Figure 4. 2 Engineering stress strain curve for weld SS 308

Table 4. 4 Tensile properties of weld SS 308

Material	YS (MPa)	UTS (MPa)	ϵ_u %	ϵ_t %
Weld SS308	408	596	48	52

4.3.2 True stress strain behaviour of weld SS 308

The true stress (σ) vs. true strain (ϵ) curve of the investigated material is presented in Fig. 4.3. The corresponding values of strain hardening exponent n and strength coefficient K were calculated using Hollomon equation $\sigma = K\epsilon^n$. The obtained results are plotted as

\ln (true stress) vs. \ln (true strain) in the post-elastic domain which results into straight lines as shown in Fig. 4.3. The values of n was estimated from the slope of the plot and the strength coefficient, K values was obtained from the intercept of this plot to the stress axis at $\epsilon = 1$.

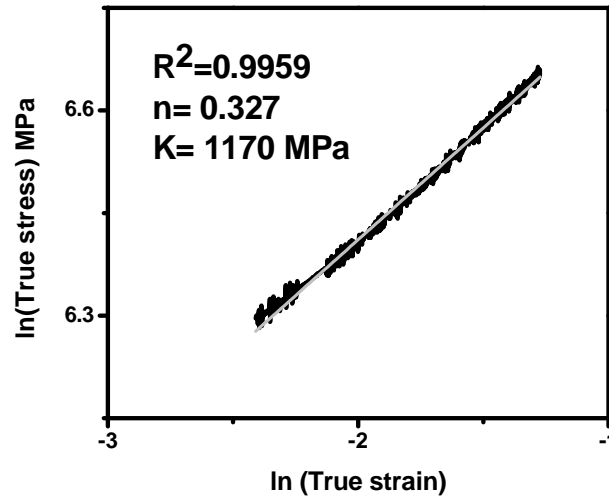


Figure 4. 3 True stress strain curve for weld SS 308

4.3.3. Fractographic analysis of tensile specimens

The fractographs of tensile specimens of weld metal are presented in Fig 4.4. The figure shows presence of dimples and micro voids which indicates the ductile mode of fracture.

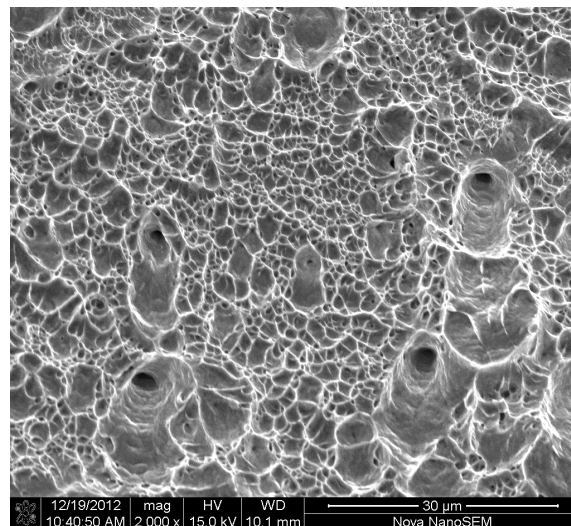


Figure 4. 4 Fractograph of post tensile weld SS 308 specimen

The micromechanism of ductile fracture consists of initiation of voids, their growth and coalescence. These voids initiate from inclusions, precipitates, second phase particles, etc., in the metallic matrix and grow further under the influence of hydrostatic stress and plastic strain [50].

4.4 Cyclic deformation behaviour of weld SS 308

This section provides us insight of materials inelastic behaviour by studying certain aspects of cyclic deformation behaviour such as Bauschinger effect, cyclic hardening/softening, cyclic stress strain curve and Masing-nonMasing behaviour etc..

4.4.1 Bauschinger effect

A material under uniaxial loading unloading regime in plastic region shows substantial decrement in reversed yield stress [51]. Therefore, the material may yield at lower stress levels during reloading in reverse direction (compression) [39]. Fig 4.5 shows typical diagram depicting Bauschinger effect. In the present investigation two established parameters i.e., Bauschinger strain and Bauschinger stress are evaluated to quantify this effect. The stress parameter ($\beta_{\sigma 1}$) to represent Bauschinger effect can be expressed as

$$\beta_{\sigma 1} = \sigma_p - \sigma_{yr} / \sigma_p$$

Where, σ_p is the maximum stress and σ_{yr} is the yield stress in reverse direction.

Bauschinger strain can be defined as the plastic strain on stress reversal at 75% of the maximum tensile stress in the forward direction.

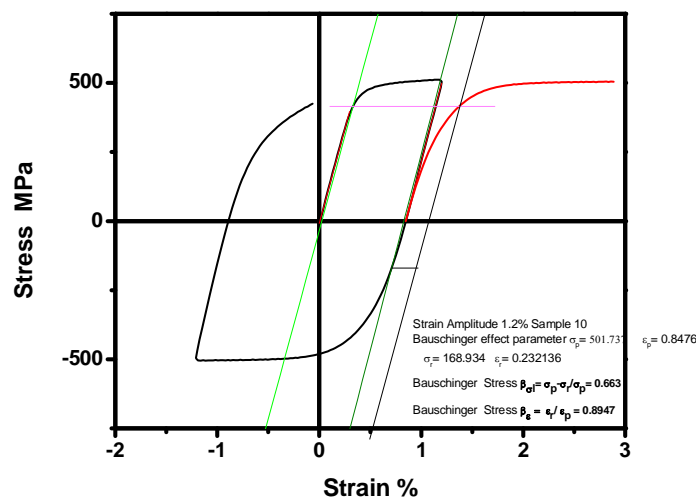


Figure 4. 5 Schematic diagram depicting Bauschinger effect

The variation of strain parameter with corresponding strain amplitude is represented in Fig 4.6.

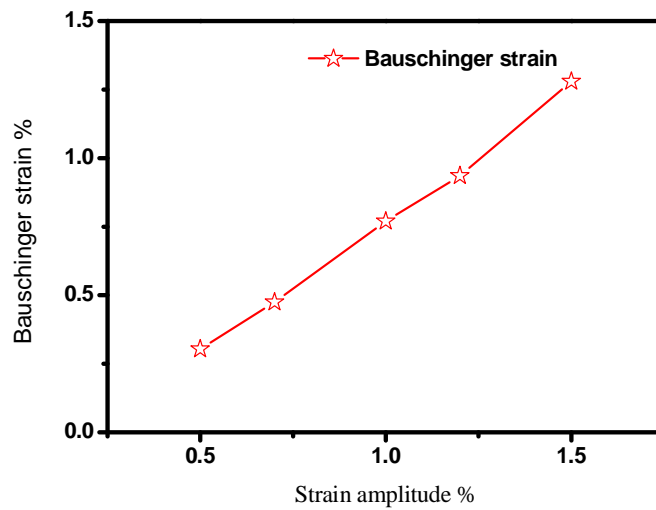


Figure 4. 6 Bauchinger strain

It can be observed that Bauschinger strain is directly proportional to strain amplitude. As reported, this is due to the presence of second phase particles (precipitates of carbide in this alloy) [52] Similar trend is also observed for AISI 304 LN and SA 333 by Paul S K, 2011[40]. The variation of Bauschinger stress with strain amplitude is represented in Fig 4.7. This shows increase in stress parameter $\beta_{\sigma 1}$ with reducing strain amplitude.

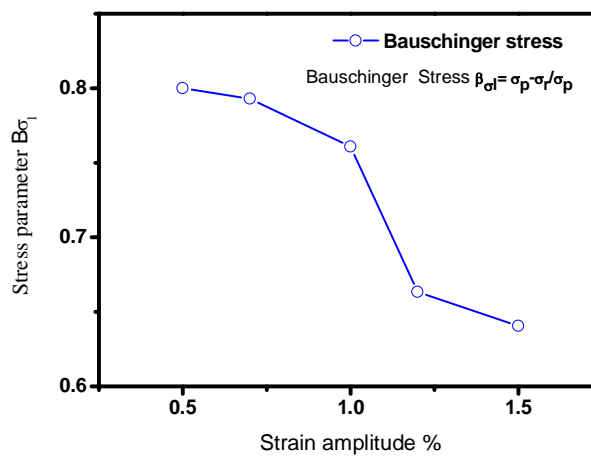


Figure 4. 7 Bauchinger stress

The mechanism involved in the process can be well explained on the basis of composite model (Masing) and internal stress theory (Heyn). The composite model states the premature yielding in soft phase in a dual phase materials. However, the internal stress theory asserts that the residual stresses developed during cyclic loading reduce yield strength of the material in opposite direction[39]

4.4.2. Cyclic hardening softening behaviour

The application of fully reversed cyclic loading exhibits certain changes in its stress strain response. Under strain controlled cyclic condition, material may exhibit hardening or softening depending upon the history of a material. Under these conditions increase or decrease in stress amplitude is observed during fatigue cycling of material. In general, hard material (cold worked) shows cyclic softening due to dislocation annihilation and soft material (annealed) exhibits cyclic hardening due to dislocation multiplication. Other variables such as nature and direction of loading, volume fraction of the phases, number of slip systems available, second phase particles etc. also play significant role in materials hardening-softening behaviour. Fig 4.8 shows different combination of initial hardening followed by softening of the metal. This may be attributed to the development of internal stresses due to non-equilibrium cooling during welding process and formation of complex microstructure consisting dendrites of delta ferrite dispersed in a matrix of austenite.

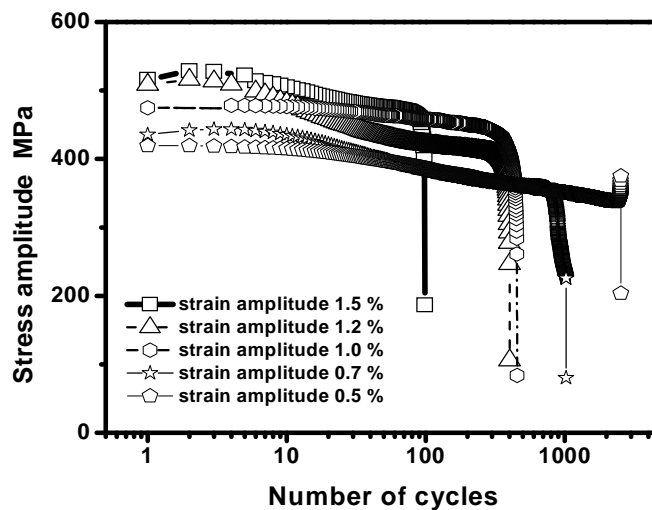


Figure 4. 8 Cyclic hardening softening behaviour

It is worth to notice that the extent of initial hardening varies with strain amplitudes. The initial hardening is moderate for strain amplitudes range 0.5%- 1.0% on the other hand, sharp initial hardening is observed in the strain amplitudes range 1.2% -1.5%. The material in all cases exhibited softening on subsequent cycling. Various researchers attributed the subsequent softening to the re-arrangement of the dislocation network and formation of stable microstructure [40]. Fig. 4.9 reports the degree of hardening/ softening with respect to strain amplitude [42]. The results indicate softening when subjected to cycling loading up to strain amplitude of 1.2 % however hardening at strain amplitude 1.5%. Similar trends are also reported in literature [42]

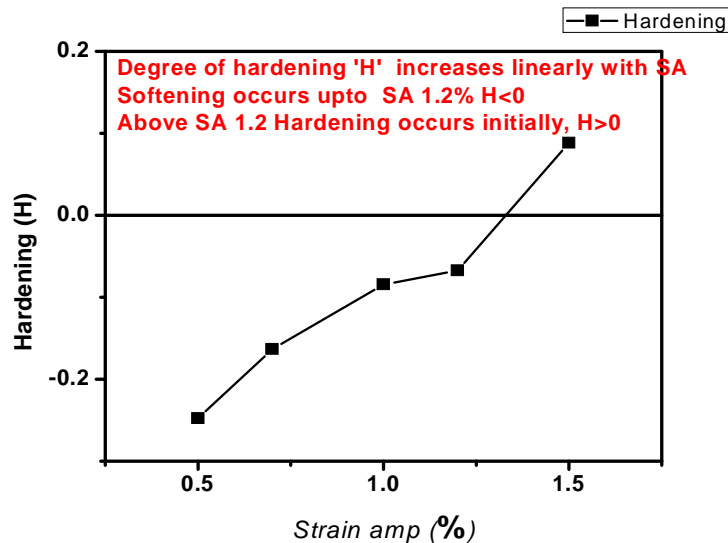


Figure 4. 9 Degree of Hardening

4.4.3 Variation of Loop shape parameter

Loop shape parameter, V_H is defined as the ratio of loop area to area of parallelogram with base $2\varepsilon_p$ and height $2\sigma_a$ [43]. V_H is presented as a function of number of strain cycles in Fig. 4.10. In this case V_H varies during fatigue cycling which corresponds to the formation of microstructures with persistent slip bands [53] It is evident that the increase in strain amplitude above 0.5% increases V_H and has a tendency to approach to 1. This

indicates increase in brittleness with increasing strain amplitude during strain controlled cycling.

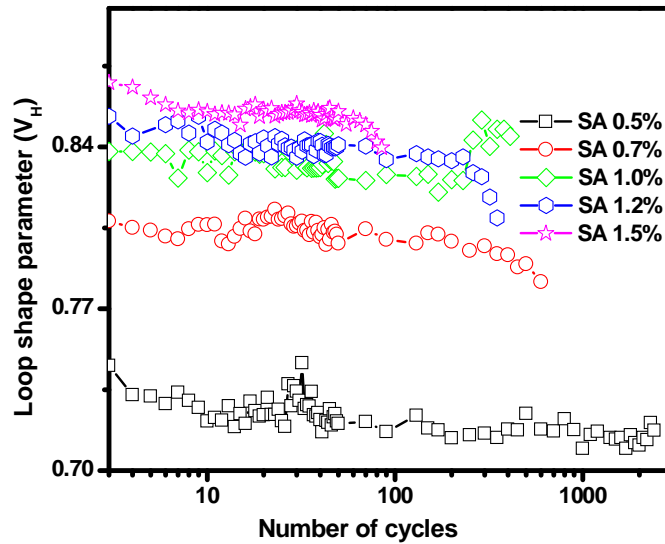


Figure 4. 10 Effect of loop shape parameter on fatigue life.

4.4.4. Stability in cyclic stress-strain

Calculation of stable loop from the stress-strain hysteresis data is one of the important aspects of LCF analysis. In half loop cycle approach the loop formed at the half life cycle is taken as stable loop, in case stability is not achieved throughout the test.

The other approach is based on derivative, $d\sigma/dN$. This derivative is plotted as a function of strain cycle and illustrated in Fig 4.11. This plot can also be used to identify the stable loop formation. The first point in stable plateau is taken as the stable cycle (loop). This approach is more appropriate as it is linked with the stability in the $d\sigma/dN$. The calculated stable loop for various strain amplitudes are tabulated in Table 4.5. This further indicates that early stability occurs with increasing magnitude of strain amplitude.

Table 4. 5 Stable loop for different strain amplitudes

Strain amplitude	N_f	Stable loop no.
± 0.5 %	2534	690
± 0.7 %	1024	266
± 1.0 %	455	295
± 1.2 %	402	145
± 1.5 %	98	52

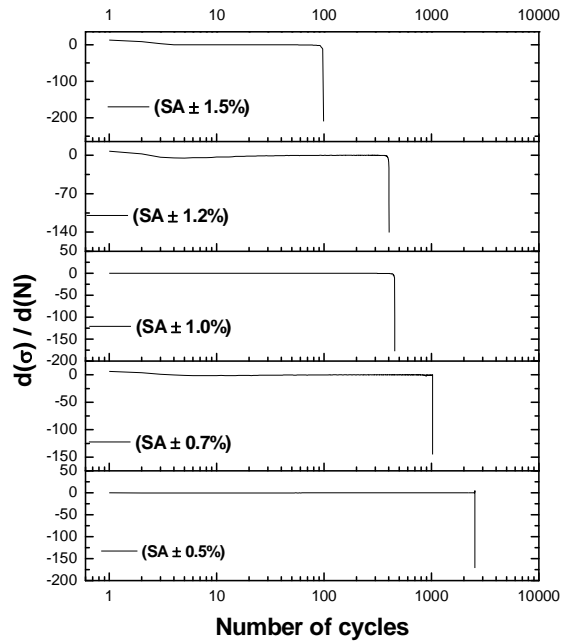


Figure 4. 11 Cyclic stability curve

4.4.5. Coffin Mansion plot

The Coffin Mansion plot i.e., plastic strain amplitude vs. number of cycles to failure plot is presented in Fig. 4.12 [37]. The estimated value of fatigue ductility coefficient (ϵ_f') and fatigue ductility exponent (c) from the figure are 1.29786 and -0.51532 respectively. These results are in line with the reported work [37].

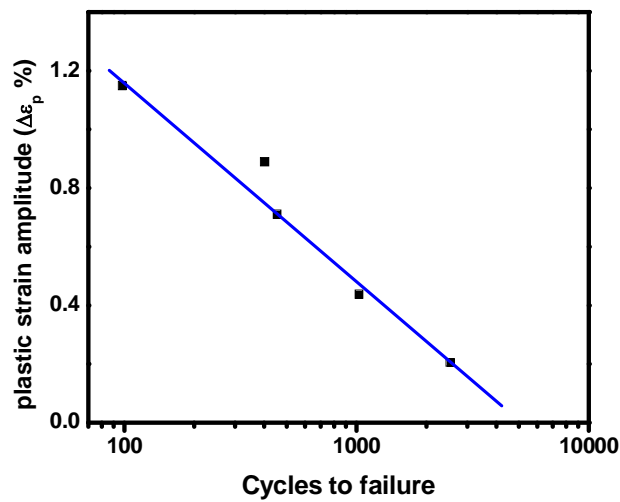


Figure 4. 12 Coffin Mansion plot

4.4.6 Variation of total energy with strain amplitude

The total energy of stable loops was calculated by simple integration. The total energy of stable loops versus strain amplitude is presented in Fig 4.13. The figure shows that the energy associated with the stable loop increases with the strain amplitude. It is worth to mention that fatigue life decreases with increasing strain amplitude.

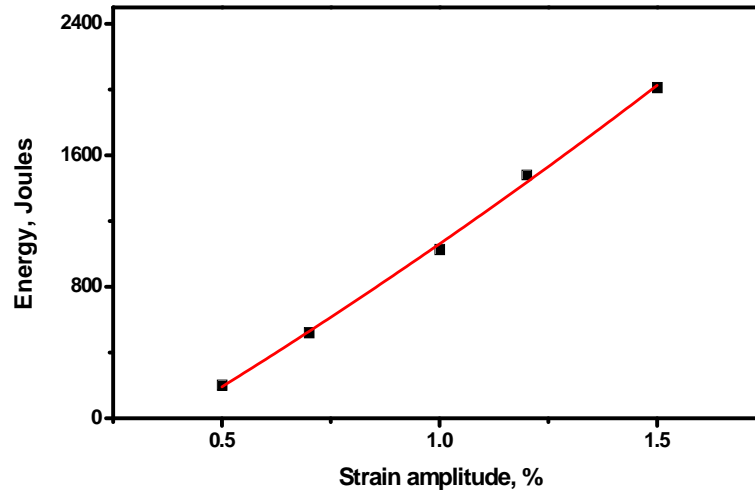


Figure 4. 13 Variation of energy absorption with fatigue life

4.4.7. Cyclic stress strain curve

Determination of cyclic stress strain curve and its comparison with monotonic stress strain curve provide quantitative assessment of the cyclically induced changes and damage in the material[37]. This plot for the material is presented in Fig. 4.14. Cyclic parameters such as cyclic strength coefficient (K') and cyclic strain hardening exponent (n') are found to be 902 MPa and 0.2046 respectively.

$$\frac{\Delta\varepsilon}{2} = \frac{\Delta\varepsilon_e}{2} + \frac{\Delta\varepsilon_p}{2} = \frac{\Delta\sigma}{2E} + \left(\frac{\Delta\sigma}{2K'}\right)^{\frac{1}{n'}} \quad [37]$$

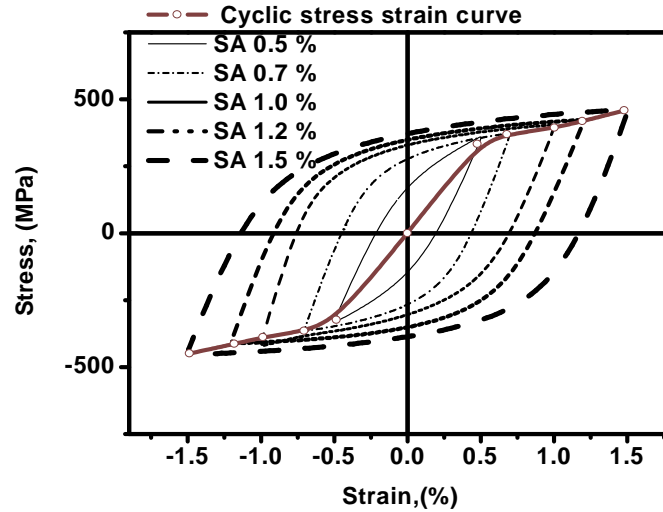


Figure 4. 14 Cyclic stress strain curve

4.4.8. Comparison of MSSC and CSSC

The cyclic stress strain curve (CSSC) and monotonic stress strain curve (MSSC) are illustrated in Fig 4.15. The comparison of CSSC to MSSC indicates complex hardening/softening behaviour, softening at lower strain amplitude and hardening at higher strain amplitude. This is an indication of variation in hardening-softening behaviour with varying strain amplitudes. In the present material softening is dominant upto strain amplitude of 1.2 % whereas hardening occurs on application of high strain amplitude. Similar behaviour is also observed by Hussain K 1993[54] in high strength steel. It is argued that dual phase materials exhibit complex behaviour.

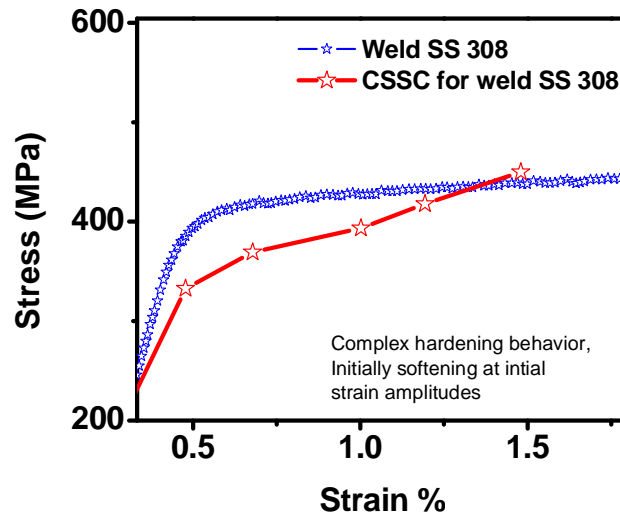


Figure 4. 15 Comparison of cyclic and monotonic stress strain curve

4.4.9. Non Masing behaviour

As discussed in Chapter 2, a material is said to be Masing-type when the hysteresis loop branches (ascending-descending ones), can be described by the cyclic stress-strain curve magnified by a factor of 2 for this type of material when the compressive tips of stable hysteresis loops of various strain amplitudes are transferred to a common origin-the maximum compressive stress-the upper branch would form a unique curve. From microscopic point of view Masing behaviour is associated with stable microstructural condition and dislocation substructure against fatigue cycles. Most steels do not shown Masing behaviour [55] Some engineering materials show Masing behaviour under certain testing conditions [55][56]. In the present investigation as shown in Fig.4.16, where the upper branches of hysteresis loops of the investigated material are displayed and does not form an unique curve. The behaviour is also depends on the amplitude of plastic strain ϵ_{ap} . Therefore, the figure shows non Masing character in present metal under the attempted loading conditions. The non-masing behaviour are observed in those metals in which cyclic deformation is controlled by the matrix properties and dislocation cells form at relatively low strain ranges typical of high stacking fault energy alloys[2].

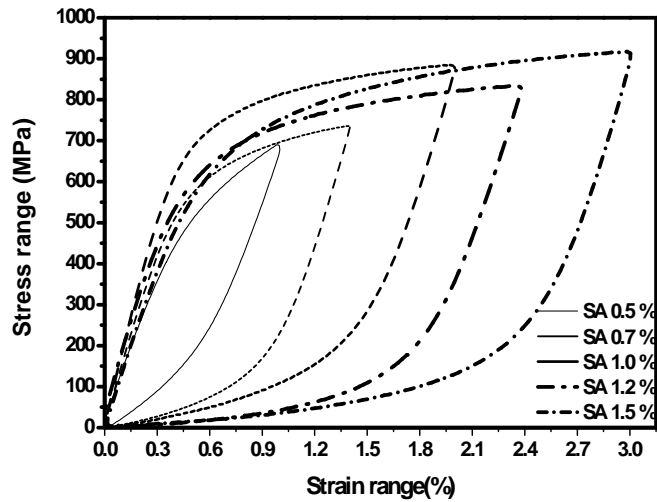


Figure 4. 16 Non Masing behaviour of material

4.4.10. Master curve

Master curves are constructed for weld SS 308 Fig 4.17 (a). Such curves are obtained by matching the loading branches of stable hysteresis loops of different strain amplitudes, by translating each loop along the linear elastic portions. The equation for the master curve corresponding to the hysteresis loop with minimum strain range (i.e., with respect to the translated axis) can be written as

$$\Delta \varepsilon^* = \frac{\Delta \sigma^*}{E} + 2 \left(\frac{\Delta \sigma^*}{2K^*} \right)^{1/n^*}$$

Where asterisk superscript indicates that the quantity is measured with respect to the translated co-ordinate system. The values of K^* and n^* are found by fitting above equation to the experimental data. The modified cyclic coefficients n^* and K^* are calculated from Fig 17 (b) and found to be 0.1549 and 907 MPa respectively. The deviation from Masing behaviour due to cyclic expansion of proportional limit is expressed by the proportional stress limit, $\delta \sigma_0$ and expressed as follows,

$$\delta \sigma_0 = \Delta \sigma - \Delta \sigma^* = \Delta \sigma - 2K^* \left(\frac{\Delta \varepsilon^*}{2} \right)^{n^*}$$

The proportionality limit $\delta\sigma_0$ was calculated using the above equation. It may be noted here that $\delta\sigma_0$ is a measure of deviation from Masing behaviour and found to be 286 MPa.

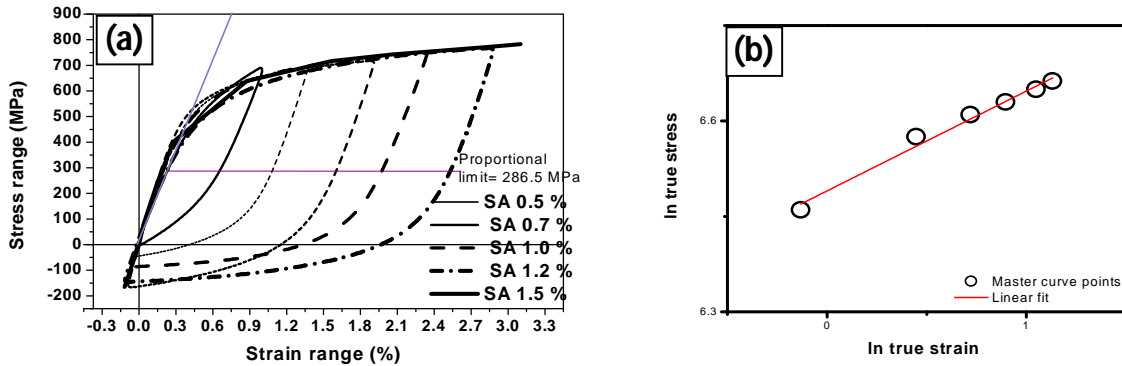


Figure 4. 17 (a) Master curve for weld SS 308 and (b) calculation of parameters from master curve

4.4.11. Variation of Plastic energy with strain amplitude

The major portion of the fatigue damage is generally caused by the plastic strain. It is therefore important to calculate the plastic strain energy (PSE) experimentally as well as with the help of the constitutive equation, following Ellyin's approach [4]. It is well understood that PSE varies from cycle to cycle. Fig 4.18 (a) shows both calculated plastic strain energy (CPSE) and experimentally determined plastic strain energy (EPSE) are in good agreement with each other. Fig 4.18 (b) suggests that at lower strain amplitude

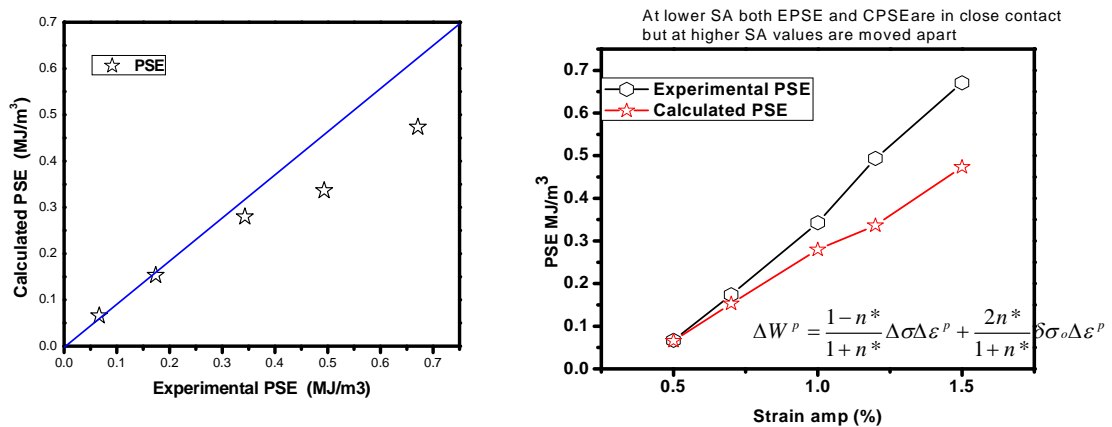


Figure 4. 18 (a) Comparison of CPSE and EPSE (b) Comparison with respect to strain amplitude

EPSE and CPSE are nearly same however with increasing strain amplitude the value of EPSE increases more rapidly than CPSE.

4.4.12 Fatigue life estimation

4.4.12.1. Walker model

As discussed in Chapter 2, Walker [3] suggest that life of the material can be predicted using equation given below,

$$\sigma_a^{eq} = \sigma_{max}^{1-\gamma} \sigma_a^\gamma = \sigma_{max} \left(\frac{1-R}{2} \right)^\gamma = \sigma_a \left(\frac{2}{1-R} \right)^{1-\gamma}.$$

Where γ is constant and considered to be the materials property and for the present alloy (as in case of steels) it is taken equal to 0.65[3]. The equivalent stress amplitude versus cycles to fail is presented in Fig 4.19.

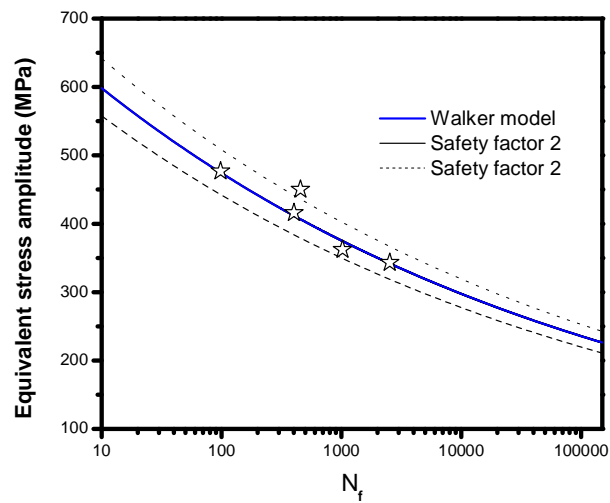


Figure 4. 19 Walker model for predicting life

4.4.12.2. Smith Watson Topper (SWT) model

Smith *et al* .suggested the following equation for calculation of equivalent stress amplitude.

$$\sigma_{eq}^{SWT} = \sqrt{\sigma_{max} \sigma_{amp}}$$

$$\sigma_{eq}^{SWT} = \sigma_{max} \sqrt{\left(\frac{1-R}{2} \right)}$$

Fig 4.20 shows variation of equivalent stress amplitude with respect to fatigue life of the material. In absence of mean stress, SWT model predicts fatigue life of the material with sufficiently high accuracy. It is also worth to note that the Walker parameter reduces to the SWT parameter if the exponent γ is 0.5. Although in the present investigation both walker and SWT (discussed below) holds good in predicting life of the material

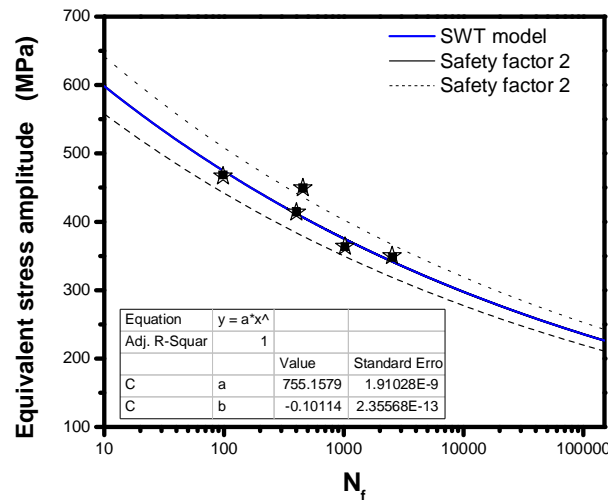


Figure 4. 20 SWT model for fatigue life prediction

Table 4.6 Comparison of walker and SWT equivalent stress.

SA	Cycle	Actual stress	Walker eq stress	% error	SWT eq stress	% error
0.5	2534	341	350.11	2.63	348.46	2.18
0.7	1024	374	363.95	2.68	363.5	2.8
1	455	406	449.35	10.5	412.5	1.47
1.2	402	411	414.05	0.98	414.5	0.85
1.5	98	474	466.54	1.57	468.93	1.06

4.4.13 Fractography

Fracture surfaces of the fatigue tested specimens were studied using scanning electron microscope. For this investigation, a set of representative fatigue specimens which failed during cyclic loading were carefully cut and the fracture surface were examined. Fractographs of specimens tested at various strain amplitudes are presented in Fig. 4.21. The presence of striations indicates the occurrence of fracture under fatigue. Fig 4.21 (f) shows a crack initiated from the surface.

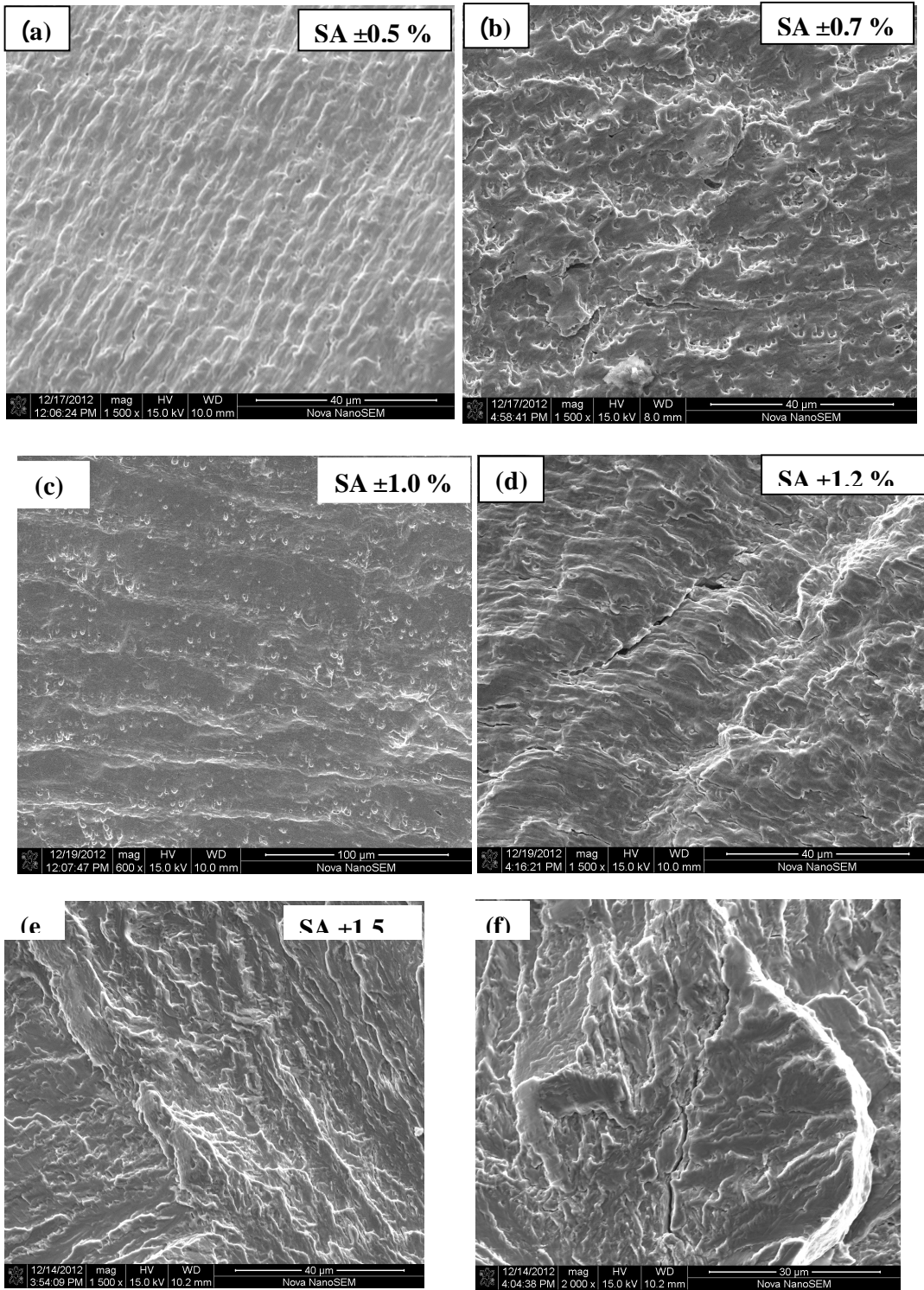


Figure 4.21 Fractographs of fracture surfaces at various strain amplitudes

Chapter 5

5.0 Conclusions and Suggestions for future work

5.1 Conclusions

5.2 Suggestion for future work

Chapter 5

Conclusions and Suggestions for future work

5.1 Conclusions

Present investigation leads to following conclusions:

- Significant directionality of strain hardening is observed in the present metal under applied strain controlled cycling indicating pronounced Bauschinger effect.
- The initial hardening and subsequent softening during strain cycling is observed in the metal.
- Hardening factor and Loop shape parameter indicate that material exhibits softening up to strain amplitude of 1.2 % and followed by hardening at higher strain amplitudes.
- Comparison of cyclic and monotonic stress strain curve conforms initial softening and subsequent hardening in the material.
- Material exhibits non Masing behaviour under present conditions.
- Calculated and experimentally determined plastic stain energy are in good agreement with each other.
- Both SWT and Walker models holds good for predicting fatigue life of the material

5.2 Scope for future work

- Low cycle fatigue behaviour of weld zone at elevated temperature of 285°C
- Optical and transmission electron microscopic studies may be useful to enhance the understanding of involved micro mechanisms.

References

- [1] ASTM E 8M, 2011, Standard test methods for tension testing of metallic materials, Annual book of ASTM standards,ASTM International.
- [2] Ellyin F. Fatigue damage crack growth and life prediction, Springer, 1996.
- [3] Dowling N E. Mean stress effects in stress-life and strain-life fatigue, ASM Internatioal, 56 (2004).
- [4] Ellyin F, Kujawski D. Plastic strain energy in fatigue, Journal of Pressure Vessel Technology, 106 (1984).
- [5] International Energy Agency, 2011, Report on Indian energy requirements, Energy Information Administration.
- [6] Miteva R, Taylor N G. General review of dissimilar metal welds in piping systems of pressurised water reactors Including WWER designs, European energy commision, 22470EN (2006).
- [7] Rie K, Portella P D. Low cycle fatigue and elasto- plastic behaviour of materials, Elsevier, 1998.
- [8] Paventhan R, Lakshminarayanan P R, Balasubramanian V. Fatigue behaviour of friction welded medium carbon steel and austenitic stainless steel dissimilar joints, Materials & Design, 32 (2011).
- [9] Cao J, Gong Y, Zhu K, Yang Z G, Luo X M, Gu F M. Microstructure and mechanical properties of dissimilar materials joints between T92 martensitic and S304h austenitic steels, Materials & Design, 32 (2011).
- [10] Arora P, Sivaprasad S. Fatigue studies on stainless steel piping materials and components : Indian AHWR, Transactions. SMIRT, BARC, Mumbai, (2011).
- [11] ANSI/ASME B36 19M, Stainless steel pipe, ASME International, 1994.
- [12] Lippold J C, Kotecki D J. Welding metallurgy and weldability of stainless steels, Canada Wiley A John, 2005.
- [13] Race J M. Carbon diffusion across dissimilar steel welds. Cambridge. 1992.
- [14] Bhattacharya D K. Failures of welded joints, Proceedings COFA-1997 NML Jamshedpur, 1 (1997).

- [15] Kuwabara K, Takahashi Y, Kawaguchi S, Fukuda Y, Fukakura J. Fatigue strength of dissimilar welded joints for the main vessel of an LMFBR, Nuclear Engineering and Design, 133 (1992).
- [16] Nelson T W, Lippold J C, Miller M J. Nature and evolution of the fusion boundary in ferritic-austenitic dissimilar weld metals Part 1-Nucleation and growth, AWS Welding Research, Oct (1999).
- [17] Celik A, Alsaran A. Mechanical and structural properties of similar and dissimilar steel joints, Material Characterisation, 5803 (1999).
- [18] Laha K, Chandravathi K S, Rao K B S, Mannan S L. An assessment of creep deformation and fracture behavior of 2.25Cr-1Mo similar and dissimilar weld joints, Metallurgical And Materials Transactions A, 32 A (2001).
- [19] Bhandari S, Dubois D, Guichard D. Behaviour of a PWR vessel dissimilar metal weld during a steam line break transient, Nuclear Engineering and Design, 207 (2001).
- [20] Faidy C, Martin G, Chapuliot S, Kayser Y, Safa N, Cipierre M F, Gilles P. Assessment of aged piping dissimilar metal weld integrity (ADIMEW), Proceedings of FISA conference, Luxembourg, (2003).
- [21] Kusko C S, Dupont J N, Marder A R. The influence of microstructure on fatigue crack propagation behavior of stainless steel welds, AWS Welding Journal, 5 (2004).
- [22] Keehan E, Effect of microstructure on mechanical properties of high strength steel weld metals, Chalmers University of Technology, 2004.
- [23] Kaçar R, Baylan O. An investigation of microstructure/property relationships in dissimilar welds between martensitic and austenitic stainless steels, Materials & Design, 35 (2004).
- [24] Ravi S, Balasubramanian V, Nemat Nasser S. Effect of mis-match ratio (MMR) on fatigue crack growth behaviour of HSLA steel welds, Engineering Failure Analysis, 11 (2004).
- [25] Lee D G, Jang K C, Kuk J M, Kim I S. Fatigue properties of inertia dissimilar friction-welded stainless steels, Journal of Materials Processing Technology, 11 (2004).
- [26] Sireesha M, Albert S K, Sundaresan S, Influence of high-temperature exposure on the microstructure and mechanical properties of dissimilar metal welds between modified 9Cr-1Mo steel and alloy 800, Metallurgical And Materials Transactions A, 36 (2005).
- [27] Cui Y, Lundin C D. Effect of microfissures on fatigue properties of austenitic stainless steel weld metals, Materials Letters, 59 (2005).

- [28] Satyanarayana V V, Madhusudhan Reddy G, Mohandas T. Dissimilar metal friction welding of austenitic–ferritic stainless steels, *Journal of Materials Processing Technology* 160 (2005).
- [29] Madhusudhan Reddy G, Mohandas T, Sambasiva Rao A, Satyanarayana V V. Influence of welding processes on microstructure and mechanical properties of dissimilar austenitic-ferritic stainless steel welds, *Materials and Manufacturing Processes*, 20 (2005).
- [30] Dupont Y J N, Kusko C S. Technical note on Martensite formation in austenitic/ferritic dissimilar alloy welds, *AWS Welding Journal*, 52 (2007).
- [31] Kim J, Lee S. A study on structural integrity of dissimilar welds in nuclear piping, *Transactions SMIRT Toronto*, 19 (2007).
- [32] Jang C, Lee J, Sung K J, Eun Jin T. Mechanical property variation within inconel 82/182 dissimilar metal weld between low alloy steel and 316 stainless steel, *International Journal of Pressure Vessels and Piping*, 85 (2008).
- [33] Kim J W, Lee K, Kim J S, Byun T S. Local mechanical properties of alloy 82/182 dissimilar weld joint between SA508 Gr.1A and F316 SS at RT and 320°C, *Journal of Nuclear Materials*, 384 (2009).
- [34] Krishnaprasad K, Prakash R V. Fatigue crack growth behavior in dissimilar metal weldment of stainless steel and carbon steel. *World Academy of Science. Engineering and Technology*, 56 (2009).
- [35] Hasan M M, Abadi M P. Correlation between macro/micro structure and mechanical properties of dissimilar resistance spot welds of AISI 304 austenitic stainless steel and AISI 1008 low carbon steel, *Association of Metallurgical Engineers of Serbia AMES*, 16 (2010).
- [36] Samal M K, Dutta B K, Kushwaha H S. A study on ductile fracture initiation in the pht piping material of an indian PHWR using local approach, *International Journal of Pressure Vessels and Piping*, 76 (1999).
- [37] Dieter G E. *Mechanical metallurgy*, MacGraw- Hill Book Company, 1996.
- [38] Suresh S. *Fatigue in materials*, Cambridge University Press, 1998.
- [39] Yan J. *Study of Bauschinger effect in various spring steels*, University of Toronto. 1998.
- [40] Paul S K. *Experimentation and material modelling for cyclic plastic deformation behavior in primary heat transport piping (PHT) materials*. Jadavpur University. Kolkata, 2011.
- [41] Shang H, Ding H J. Low cycle fatigue stress-strain relation model of cyclic hardening or cyclic softening factor, *Engineering Fracture Mechanics*, 54 (1996).

- [42] Ye D, Matsuoka S, Nagashima N, Suzuki N. The low-cycle fatigue, deformation and final fracture behaviour of an austenitic stainless steel, *Materials Science and Engineering A*, 415 (2006).
- [43] Polák J, Obrtlík K, Hajek M. Cyclic plasticity in type 316L austenitic stainless steel, *Fatigue Fracture Engineering Material Structures*, 17 (1994).
- [44] Morrison D J, Jia Y, Moosbrugger J C. Cyclic plasticity of nickel at low plastic strain amplitude. hysteresis loop shape analysis, *Materials Science and Engineering A*, 314 (2001).
- [45] Dutta K. Accumulation of ratcheting strain in polycrystalline metallic materials, IIT Kharagpur, 2012.
- [46] Branco R, Costa J D, Antunes F V. Low-cycle fatigue behaviour of 34CrNiMo6 high strength steel, *Theoretical and Applied Fracture Mechanics*, 58 (2012).
- [47] ASTM E 384, 2011, Standard test method for knoop and vickers hardness of materials, Annual book of ASTM standards, ASTM International.
- [48] ASTM E 606, 2011, Standard practice for strain-controlled fatigue testing. Annual book of ASTM standards, ASTM International.
- [49] David S A, Vitek J M, Alexander D J. Embrittlement of austenitic stainless steel welds, 1995.
- [50] Das A, Tarafder S. Geometry of dimples and its correlation with mechanical properties in austenitic stainless steel, *Scripta Materialia*, 59 (2008).
- [51] Neel C G, Bobet V, Clavel M. Cyclic deformation behaviour and Bauschinger effect in ductile cast iron, *Materials Science and Engineering A*, 272 (2008).
- [52] Plumtree A, Raouf H A. Cyclic stress strain response and substructure, *International Journal of Fatigue*, 23 (1998).
- [53] Saad A A. Cyclic plasticity and creep of power plant materials, University of Nottingham, 2012.
- [54] Hussain K. Monotonic and cyclic stress strain behavior of a high strength steel, *Metallurgical Science and Technology*, 11 (1993).
- [55] Jiang Y, Zhang J. Benchmark experiments and characteristic cyclic plasticity deformation. *International Journal of Plasticity*, 24 (2008).
- [56] Halama R, Sedlak J, Sofer M. Phenomenological modelling of cyclic plasticity. Intech International, 1 (2012).
- [57] Dutta A, Material characterisation of SS316 for low cycle fatigue damage, Jadavpur University, (2009)

BIO-DATA

Name Abhishek Chaturvedi
Date of birth 04.05.1988
Permanent Address Bewar road, Bholepur, Fatehgarh
Disst- Farrukhabad Uttar Pradesh, 209625
E-mail ID abhishek.mse@gmail.com
Languages Known Hindi, English

EDUCATIONAL QUALIFICATION

Examination	Discipline/ Specialization	School/college	Board/ University	Year of Passing	Percentile
M. Tech (Research)	Metallurgical and Materials Engineering	NIT Rourkela	National Institute of Technology Rourkela	2013	9.12* (CGPA)
B. Tech.	Metallurgical and Materials Engineering	UIET, CSJM University kanpur.	CSJM University	2010	8.45 (CGPA)
HSSC	Maths, Physics, Chemistry	Central School Fatehgarh	CBSE	2005	62 %
HighSchool		Central School Fatehgarh.	CBSE	2003	78 %

PROJECT DETAILS

M. Tech (Research)

Low Cycle Fatigue Behaviour of AISI 308 Stainless Steel Weld Metal

Conference

- A Chaturvedi, B B Verma, N Narasaiah, A Das, H N Bar, S Shivaprasad; National conference on processing and characterization of materials organized by NIT Rourkela in November 2011 held at Rourkela India

- A Chaturvedi, B B verma, N Narasaiah, S Sivaprasad, H N Bar; poster presentation at National Metallurgical Day (NMD), in November 2012 held at Jamshedpur, India.

- A Chaturvedi, B B verma, N Narasaiah, S Sivaprasad, H N Bar; Fatigue fracture and integrity assessment (FFIA) organized by Tata Steel in May 2012 held at Jamshedpur, India.